INT. REVIEWS IN PHYSICAL CHEMISTRY, 2000, VOL. 19, NO. 3, 409–453

Shape and size dependence of radiative, non-radiative and photothermal properties of gold nanocrystals

STEPHAN LINK and MOSTAFA A. EL-SAYED†

Laser Dynamics Laboratory, School of Chemistry and Biochemistry, Georgia Institute of Technology, Atlanta, GA 30332-0400, USA

Driven by the search for new materials with interesting and unique properties and also by the fundamental question of how atomic and molecular physical behaviour develops with increasing size, the field of nanoparticle research has grown immensely in the last two decades. Partially for these reasons, colloidal solutions of metallic (especially silver and gold) nanoparticles have long fascinated scientists because of their very intense colours. The intense red colour of colloidal gold nanoparticles is due to their surface plasmon absorption. This article describes the physical origin of the surface plasmon absorption in gold nanoparticles with emphasis on the Mie and also the Maxwell-Garnett theory and reviews the effects of particle size and shape on the resonance condition. A better understanding of the relationship between the optical absorption spectrum (in particular, the plasmon resonance) and such particle properties as its dimensions or surrounding environment can prove fruitful for the use of the plasmon absorption as an analytical tool. The plasmon resonance has also had a great impact on the Raman spectrum of surface-adsorbed molecules and a large enhancement of the fluorescence quantum yield of gold nanorods is observed. Furthermore, following the changes in the plasmon absorption induced by excitation (heating) with ultrashort laser pulses allows one to monitor the electron dynamics (electron–electron and electron–phonon interactions) in real time, which is important in understanding such fundamental questions regarding the thermal and electrical conductivity of these nanoparticles. Very intense heating with laser pulses leads to structural changes of the nanoparticles (nuclear rearrangements in the form of melting and fragmentation).

Contents

† Author for correspondence. E-mail: mostafa.el-sayed@chemistry.gatech.edu.

International Reviews in Physical Chemistry ISSN 0144-235X print/ISSN 1366-591X online
http://www.tand.co.uk/journals

1. Introduction

Over the last two decades the interest in colloidal and cluster chemistry has grown significantly [1–14]. The more general term nanoparticle includes small clusters or giant molecules (fewer than 100 atoms in the size range around 1 nm) and larger particles consisting of tens to hundreds of thousands of atoms (or even greater) and having a diameter in the range of tens to hundreds of nanometres. The latter kind of material has long been known to scientists as colloids [1, 2, 4, 12, 15–17], most often referring to suspensions of metal particles in an aqueous medium. In fact, colloidal gold has been used as a colouring pigment dating back to the middle ages [15]. In the nineteenth century, Faraday [18] already recognized that the ruby red colour of colloidal gold stems from the presence of aggregates of gold atoms although he had no means of analysing the size of these gold nanoparticles by modern analytical techniques such as transmission electron microscopy (TEM).

Around the turn of the twentieth century, the field of colloidal chemistry was undergoing tremendous growth due to the pioneering contributions from Ostwald and Mie and the Nobel Prize winners Svedberg and Zsigmondy. The work by Mie [19], who first explained the origin of the red colour of gold nanoparticles, will be discussed in greater detail in this review article. The one thing that all these pioneers had in common was the fact that they realized how dramatically the ratio of surface atoms to interior atoms changes if one successively divides a macroscopic object (e.g. a cube) into smaller parts. The study of the accompanying changes in the physical chemistry of nanoscale material compared with the bulk or to individual atoms was their goal then, as it still is today.

As an example of how drastically the number of surface atoms increases with decreasing particle size, consider a cube of iron 1 cm on an edge. The percentage of surface atoms would be only $10^{-5}\%$. Dividing the same cube into smaller cubes with an edge of just 10 nm results in a percentage of surface atoms of 10% and in a cube with an edge of 1 nm every atom would be a surface atom. This might illustrate why changes in the size range of a few nanometres are expected to lead to great changes in the physical and chemical properties of the nanoparticle. The investigation of new material properties is interesting from a technological standpoint [12–14, 20]; the transition from individual atoms to the bulk state of matter is, however, also of very great fundamental importance in science [21–26].

The reason for the resurrection of colloid and cluster science in recent years is that the gap between the organometallic clusters and small colloidal particles has been closed by synthesis of larger clusters stabilized by organic ligands [12]. At the same

time, size selective separation methods of colloidal particles have allowed the isolation of smaller clusters from the large distribution of sizes [27–29]. In fact the monodispersity of the particle size is a key factor in enabling the study of size-dependent physical properties of the nanoparticles. In this way, particles can be isolated in a quantity which easily allows one to use less sensitive analytic techniques than usually employed in a cluster beam experiment. Not only have the chemical preparation methods improved significantly, but also the progress in computing capabilities [12, 23] makes it now possible to calculate cluster properties of fairly large particles from first principles similar to calculations of molecular properties. On the other hand, band structure calculations in solid-state physics do not have to involve infinite boundary conditions any more as the significance of a finite size can be taken into account. Therefore, the fact that the areas of cluster and colloid science are merging together with the advancement in the chemical synthesis techniques explains and justifies the use of the word *nanoparticle* for all particles falling in the size regime of 10^{-9} m.

The reason for studying nanostructured materials from a technological standpoint is mainly the anticipated applications in optical systems and catalysis [12–14, 20]. In particular, in the fields of optical data communication and optical data storage the need for new materials with high nonlinearities is driving nanoparticle research. The ease of tuning the optical properties gradually with particle size and shape have made nanoparticles very interesting compared with organic dye molecules [3]. Semiconductor nanoparticles have already been successfully used in solar cells converting sunlight into electricity [20]. On the other hand, because of their high surface-to-volume ratios, metal nanoparticles (especially platinum and palladium) are important as catalysts [12]. Shape control over platinum nanoparticles [30] might allow the exposure of different crystal surfaces for catalysis showing differences in catalytic efficiency.

In general, nanoparticles can be composed of metals in their neutral valence state or as their oxides, sulphides, selenides, etc. Nanoparticles composed of a semiconducting material are of great interest since their bandgap transition has moved to the visible compared with the infrared for the bulk [3, 9, 10]. Even though this article will focus on metallic nanoparticles, all the particles have in common that they must be stabilized by molecules attached at their surface (to control their size and to prevent them from agglomeration and precipitation) or must be embedded in a solid matrix in order to avoid aggregation and the formation of the thermodynamically favoured bulk material. In the absence of any counteractive repulsive forces the van der Waals forces between two metal nanoparticles would lead towards coagulation. This can be avoided by either electrostatic or steric stabilization [12]. Electrostatic stabilization is realized by an electrical double layer arising from the attraction of negatively charged ions to the (mainly) metal nanoparticles. The positive counterions then form a second layer (hence the electrical double layer). Steric stabilization in solution is achieved by binding of polymers or surfactant molecules with long alkyl chains to the particle surface. The long chains of the organic molecules prevent the particles from coming close to each other. The surface organic molecules further prevent the oxidation of the neutral metal in solution and small nanoparticles of gold can be isolated as a powder and are completely stable against air oxidation [31]. In the case of gold, organic thiols have been employed very successfully in the synthesis of small gold clusters [28, 31, 32]. The gold–thiolate bond is known to be particularly strong and allows the isolation of these compounds as molecular substances.

Preparation methods of metallic nanoparticles range from chemical methods to metal vapour synthesis [12]. The most widely used and oldest method is reduction of the metal salt in solution by reducing agents such as sodium citrate, phosphor, sodium borhydride or hydrogen [33]. While sodium citrate used in an excess can also serve as a protective capping agent, in the case of the other mentioned substances, polymers or surfactants have to be added before the salt reduction in order to stabilize the nanoparticles. The reduction with sodium citrate has been worked out in detail by Turkevich and co-workers [34–37] and produces gold nanoparticles with an average diameter of about 20 nm with a very narrow size distribution and good reproducibility. It is therefore often used to prepare gold nanoparticles in solution which have been widely used as labelling agents in biological samples using TEM [5].

Another reducing agent of a different kind employed very successfully is the use of free electrons or radicals generated in solution by radiolytic techniques [1, 2]. Henglein [1, 2] and Mulvaney [4] have used a γ-ray source to produce a wide variety of different metal nanoparticles from cadmium, thallium and lead, to silver and gold. Thermolysis [38–41] and photolysis [42] of unstable organometallic precursors is another preparation method, which has been used for the synthesis of palladium and platinum nanoparticles. Electrolysis [43, 44] can also be used to prepare metal nanoparticles. In metal vapour synthesis [45], atomic metal vapour is simply condensed in a dispersing medium at low temperatures (because of the reactivity towards water this is exclusively done in organic solvents). Furthermore, nanoparticles can be grown in optically transparent glasses at high temperatures [46], which is often the procedure most widely used in solid-state physics. In order also to synthesize nanoparticles of a certain shape, the reduction of the metal precursors can be carried out in a constraint environment such as the inside of zeolites [12], porous alumina [47–52] and micelles [44, 53–55].

The feature that distinguishes the preparation methods listed above from each other in obtaining a homogeneous size distribution is the rate of nuclei formation where the nuclei are homogeneously distributed over the reaction volume. This allows all clusters to grow with the same rate and one obtains a kinetically favoured product rather than reaching the thermodynamically most favourable state (which would of course be the bulk metal itself if given enough time).

While it would be worth reviewing the wide field of preparation methods more thoroughly, the above discussion is used here only to serve as a general introduction. Instead, this article focuses on the optical properties of the noble metal nanoparticles, which show a pronounced surface plasmon absorption. The exact preparation methods are of less importance for the main optical absorption feature. It should, however, be mentioned that the results presented here are all obtained on gold nanoparticles produced either by the citrate method [34, 35, 56] or by an electrochemical method with the use of organic surfactant molecules producing gold nanorods [44, 53]. TEM pictures of 48 nm nanodots and gold nanorods with a mean aspect ratio of 3·3 are shown in figures 1(*a*) and (*b*) respectively. The effect of the surrounding medium will be discussed at appropriate times throughout the text. The first part of this review discusses the physical origin of the surface plasmon absorption and the effects of size and shape on the resonance condition. The theories developed by Mie [19] and Maxwell-Garnett [57] early in the twentieth century will be outlined in more detail. The second part deals with the optical response of the surface plasmon band after excitation with a femtosecond laser pulse. Time-resolved transient absorption spectroscopy allows direct observation of the electron dynamics as the electrons couple to the lattice. Very intense laser heating, on the other hand, leads to

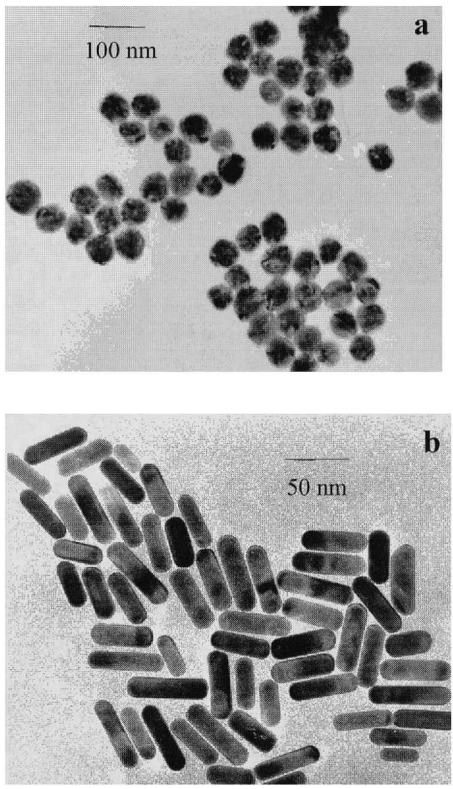

Figure 1. TEM images of (*a*) spherical gold nanoparticles with an average diameter of 48 nm and (*b*) gold nanorods with a mean aspect ratio of 3·3.

nuclear rearrangements and permanent shape transformation of the nanoparticles. This transformation can also be followed directly by monitoring the surface plasmon absorption. We shall see that TEM analysis is of crucial importance in order to correlate the structural changes with the optical absorption data.

2. Optical absorption properties of metal nanoparticles: the surface plasmon resonance

2.1. *The Mie theory*

It was mentioned in the introduction that a reduction in particle size leads to different physical and especially optical properties [1–3, 8–11, 23, 58–60]. Reducing the size of the nanoparticle has a pronounced effect on the energy level spacing as the system becomes more confined. Similar to a particle in a box, the energy separation between adjacent levels increases with decreasing dimensions. This is most pronounced for semiconductor nanoparticles where the bandgap energy increases with decreasing size and the onset of the bandgap transition is shifted to higher frequencies [3, 8–10, 24–26, 61]. Since the exciton radius is typically 2–8 nm for II–VI semiconductors, particles of several nanometres in diameter are expected to undergo the transition from the bulk to the quantum-confined state. Quantum size effects are also known for metal nanoparticles [21, 22]. In order to observe the localization of the energy levels the size must be well below 2 nm as the level spacing has to exceed the thermal energy (about 26 meV). There is a simple explanation for this fundamental difference. In a

semiconductor, the interesting level spacing is the energy difference between the completely filled valence band and the empty conduction band, which corresponds to the interband transition. This energy separation is of the order of a few electronvolts and increases rapidly with decreasing size [61]. In a metal, the conduction band is half-filled and the density of energy levels is so high that a noticeable separation in energy levels within the conduction band (intraband transition) is only observed when the nanoparticle is made up of just a few atoms ($N = 100$). In fact the level spacing of the one electron states can be roughly approximated by E_F/N [21–23] where the Fermi energy E_F is typically of the order of 5 eV in most metals. A 10 nm gold nanoparticle consisting of roughly 30 000 atoms would therefore have an energy level spacing of only 0.167 meV. On the other hand, this simple approximation translates into a transition energy of 167 meV for a 30-atom cluster, which exceeds the thermal energy. Experimentally, an increased bandgap between the lowest unoccupied (molecular) orbital (LUMO) and the highest occupied (molecular) orbital has been found to be around 1.7 eV or 730 nm for a 28-atom gold cluster [62].

The surface plasmon resonance is the coherent excitation of all the 'free' electrons within the conduction band, leading to an in-phase oscillation [1, 4, 58–60]. The surface plasmon resonance does not give rise to the most intense absorption for very small clusters but is rather strongly damped [23, 63–65]. For the larger particles of several tens of nanometres in which their size is still small compared with the wavelength of light, excitation of the surface resonance can take place with visible light. For the same particles, the volume plasmon is located at very high energies (6–9 eV) [23]. The surface obviously plays a very important role for the observation of the surface plasmon resonance as it alters the boundary conditions for the polarizibility of the metal and therefore shifts the resonance to optical frequencies. In this sense, the surface plasmon absorption is a small particle (or thin layer) effect but definitely is not a quantum size effect.

Figure 2(*a*) shows how one can picture the creation of a surface plasmon oscillation in a simple manner. The electric field of an incoming light wave induces a polarization of the (free) conduction electrons with respect to the much heavier ionic core of a spherical nanoparticle. The net charge difference occurs at the nanoparticle boundaries (the surface) which in turn acts as a restoring force. In this manner a dipolar oscillation of the electrons is created with period T. Figure 2(*b*) shows the surface plasmon absorption of 22, 48 and 99 nm gold nanoparticles [56] prepared in aqueous solution by the reduction of gold ions with sodium citrate [34, 35]. The absorption spectra of the different particles are normalized at their surface plasmon absorption maximum for comparison. The molar extinction coefficient is of the order of $1 \times 10^9\ M^{-1}\ cm^{-1}$ for 20 nm nanoparticles and increases linearly with increasing volume of the particles [11]. Note that these extinction coefficients are three to four orders of magnitude higher than those for the very strong absorbing organic dye molecules. From figure 2(*b*) it can be seen that the surface plasmon absorption red shifts with increasing size while the bandwidth increases in the size region above 20 nm [56]. These trends for particles of different sizes will be discussed theoretically in the following paragraphs.

Dating back to 1908, Mie [19] was the first to explain the red colour of gold nanoparticle solutions. He solved Maxwell's equation for an electromagnetic light wave interacting with small spheres having the same macroscopic frequency-dependent material dielectric constant as the bulk metal. The solution of this electrodynamic calculation with appropriate boundary conditions for a spherical

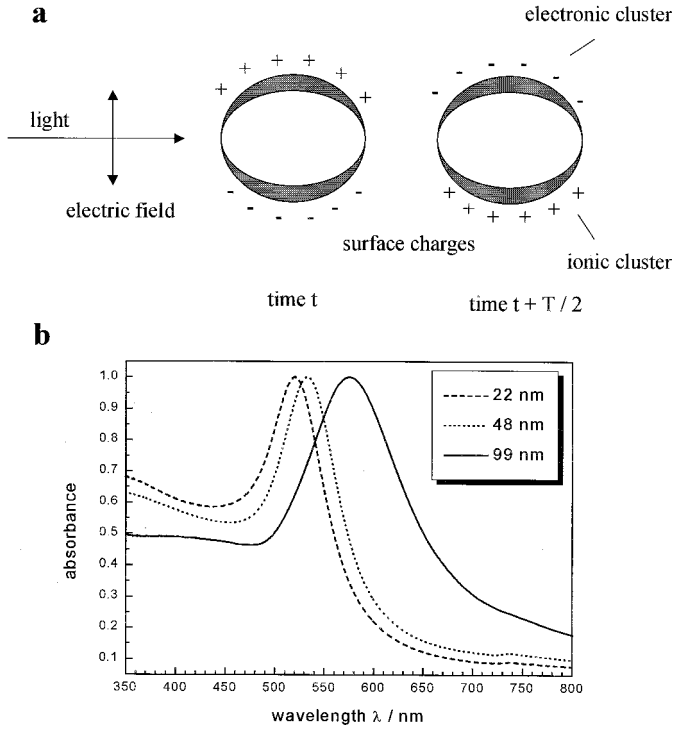

Figure 2. Surface plasmon absorption of spherical nanoparticles and its size dependence. (*a*) A scheme illustrating the excitation of the dipole surface plasmon oscillation. The electric field of an incoming light wave induces a polarization of the (free) conduction electrons with respect to the much heavier ionic core of a spherical gold nanoparticle. A net charge difference is only felt at the nanoparticle boundaries (surface) which in turn acts as a restoring force. In this way a dipolar oscillation of the electrons is created with period T. This is known as the surface plasmon absorption. (*b*) Optical absorption spectra of 22, 48 and 99 nm spherical gold nanoparticles. The broad absorption band corresponds to the surface plasmon resonance.

object leads to a series of multipole oscillations for the extinction cross-section of the nanoparticles [23, 58–60]. By series expansion of the involved fields into partial waves, one obtains the following expressions for the extinction cross-section σ_{ext} and scattering cross-section σ_{sca} [23]:

$$\sigma_{\text{ext}} = \frac{2\pi}{|k|^2} \sum_{L=1}^{\infty} (2L+1)\,\text{Re}\,(a_L + b_L), \tag{2.1}$$

$$\sigma_{\text{sca}} = \frac{2\pi}{|k|^2} \sum_{L=1}^{\infty} (2L+1)\,(|a_L|^2 + |b_L|^2), \tag{2.2}$$

with $\sigma_{\text{abs}} = \sigma_{\text{ext}} - \sigma_{\text{sca}}$ and

$$a_L = \frac{m\psi_L(mx)\,\psi'_L(x) - \psi'_L(mx)\,\psi_L(x)}{m\psi_L(mx)\,\eta'_L(x) - \psi'_L(mx)\,\eta_L(x)}, \quad b_L = \frac{\psi_L(mx)\,\psi'_L(x) - m\psi'_L(mx)\,\psi_L(x)}{\psi_L(mx)\,\eta'_L(x) - m\psi'_L(mx)\,\eta_L(x)},$$

$m = n/n_{\text{m}}$, where n is the complex refractive index of the particle and n_{m} the real refraction index of the surrounding medium. k is the wave-vector and $x = |k|r$ with r

being the radius of a nanoparticle. ψ_L and η_L are the Ricatti–Bessel cylindrical functions. The prime indicates differentiation with respect to the argument in parentheses. L is the summation index of the partial waves. $L = 1$ corresponds to the dipole oscillation as illustrated in the figure 2(*a*) while $L = 2$ is associated with the quadrupole oscillation and so on.

For nanoparticles much smaller than the wavelength of light ($2r \ll \lambda$, or roughly $2r < \lambda_{max}/10$) only the dipole oscillation contributes significantly to the extinction cross-section [1, 4, 23, 58–60]. The Mie theory then reduces to the following relationship (dipole approximation):

$$\sigma_{ext}(\omega) = 9\frac{\omega}{c}\varepsilon_m^{3/2} V \frac{\varepsilon_2(\omega)}{[\varepsilon_1(\omega)+2\varepsilon_m]^2+\varepsilon_2(\omega)^2}, \tag{2.3}$$

where V is the particle volume, ω is the angular frequency of the exciting light, c is the speed of light, and ε_m and $\varepsilon(\omega) = \varepsilon_1(\omega)+i\varepsilon_2(\omega)$ are the dielectric functions of the surrounding medium and the material itself respectively. While the first is assumed to be frequency independent, the latter is complex and is a function of energy. The resonance condition is fulfilled when $\varepsilon_1(\omega) = -2\varepsilon_m$ if ε_2 is small or weakly dependent on ω [23].

The above equation has been used extensively to explain the absorption spectra of small metallic nanoparticles in a qualitative as well as quantitative manner [23, 63]. However, for larger nanoparticles (greater than about 20 nm in the case of gold) where the dipole approximation is no longer valid, the plasmon resonance depends explicitly on the particle size as x is a function of the particle radius r. The larger the particles become, the more important are the higher-order modes as the light can no longer polarize the nanoparticles homogeneously. These higher-order modes peak at lower energies and therefore the plasmon band red shifts with increasing particle size [23, 58–60]. At the same time, the plasmon bandwidth increases with increasing particle size. This is illustrated experimentally from the spectra shown in figure 2(*b*). It also follows from the Mie theory. As the optical absorption spectra depend directly on the size of the nanoparticles, this is regarded as an extrinsic size effects [23].

The plasmon bandwidth can be associated with the dephasing of the coherent electron oscillation [56, 66–73]. Large bandwidth corresponds to rapid loss of the coherent electron motion. Electron dephasing times of a few femtoseconds are computed from the surface plasmon bandwidth, which strongly suggests that the main relaxation process involves electron–electron collisions [56]. If one assumes a simple two-level model for the plasmon absorption, the width Γ is then given by [66]

$$\frac{1}{T_2} = \pi c \Gamma = \frac{1}{2T_1}+\frac{1}{T_2^*}. \tag{2.4}$$

T_1 describes the population relaxation time (involving both radiative and non-radiative processes), T_2 is the total dephasing time and T_2^* is the pure dephasing time. The latter results from collisions that change the plasmon wave-vector but not its energy. Often T_2^* is much shorter than the energy relaxation T_1 and thus determines the value of T_2.

Assuming a homogeneous size distribution and therefore homogeneous line broadening, the total dephasing time can be computed from the measured width of the plasmon absorption band. Using equation (2.4) with the spectra shown in figure 2(*b*),

dephasing times of 4.1, 3.9 and 2.6 fs are calculated for the 22, 44 and 99 nm gold particles respectively [56]. Kreibig *et al.* [67] determined dephasing times of 2 fs for 2 nm silver clusters embedded in a matrix and 7 fs for the same clusters in vacuum (naked clusters). These extremely fast dephasing times are in agreement with nonlinear frequency mixing studies on gold nanoparticles by Heilweil and Hochstrasser [66]. They found that both T_1 and T_2 are shorter than 48 fs. More recent nonlinear studies came to the conclusion that the dephasing time of the coherent plasmon oscillation is shorter than 20 fs [68]. These results also agree with studies on lithographically produced gold and silver nanoparticles (about 200 nm in size) [70–72], for which dephasing times of 6 and 10 fs were measured by second-order nonlinear autocorrelation femtosecond spectroscopy [72]. Furthermore, recent single nanoparticle investigations with a scanning near-field optical microscope found a homogeneous linewidth of only 160 meV for some individual particles corresponding to a dephasing time of 8 fs for 40 nm gold nanoparticles in a sol–gel TiO_2 matrix [73].

The situation concerning the size dependence of the optical absorption spectrum is more complicated for smaller nanoparticles for which only the dipole term is important. As can easily be seen from equation (2.3), the extinction coefficient does not depend on the particle dimensions, which would imply that the surface plasmon absorption becomes size independent for particles smaller than about 20 nm. A size dependence is observed experimentally [4, 11, 23, 63]. For 5 nm particles the plasmon oscillation is strongly damped and its absorption becomes weak and broad and it completely disappears for nanoparticles less than about 2 nm in diameter [32, 64, 65]. This is because the electron density in the 'conduction' band becomes very small. Obviously, the assumption of bulk-like electronic bands and bulk electronic and optical properties associated with the electronic structure of the nanoparticles is rather questionable. In particular, the use of the bulk dielectric constant which enters the Mie equation as the only material-related physical quantity is not justified any longer [4, 23, 63]. However, as the Mie theory has been very successful in describing the optical absorption spectra of metal nanoparticles [4, 23, 58–60], the theory was modified in a way to account for the size effects rather than abandon it altogether.

In almost all the many theoretical models published it is assumed that the dielectric constant of the material is size dependent ($\varepsilon(\omega, r)$) below an average particle diameter of about 20 nm [23, 63]. In one of the early approaches, Kreibig and von Fragstein [74] and Kreibig [75] proposed that electron–surface scattering must be enhanced in those small particles since the mean free path of the conduction electrons is limited by the physical dimension of the nanoparticle. The mean free path of the electrons in silver and gold is of the order of 40–50 nm [76]. If the electrons scatter with the surface in an elastic but totally random way, the coherence of the overall plasmon oscillation is lost. Inelastic electron–surface collisions would also change the phase. The smaller the particles, the faster the electrons reach the surface of the particles. The electrons can then scatter at the surface and lose the coherence more quickly than in a larger nanoparticle. As a consequence the plasmon band width increases with decreasing nanoparticle radius. Indeed, it was shown theoretically [63, 74, 75] and experimentally [46, 74, 75, 77, 78] that the plasmon band width is inversely proportional to the particle radius.

Following the model of the reduction of the effective electron mean free path and enhanced electron–surface scattering [74, 75], the mathematical formulation of this problem explaining the correct size dependence of the surface plasmon absorption starts with writing the dielectric function as a combination of an interband term $\varepsilon_{IB}(\omega)$

and a Drude term $\varepsilon_D(\omega)$ considering only the free conduction electrons ($\varepsilon(\omega) = \varepsilon_{IB}(\omega) + \varepsilon_D(\omega)$). The latter is given within the free-electron model by the following expression [76]:

$$\varepsilon_D(\omega) = 1 - \frac{\omega_p^2}{\omega^2 + i\gamma\omega}, \tag{2.5}$$

where $\omega_p^2 = ne^2/\varepsilon_0 m_{eff}$ is the bulk plasmon frequency expressed in terms of the free electron density n and the electron charge e. ε_0 is the vacuum permittivity and m_{eff} the electron effective mass. γ is introduced as a phenomenological damping constant. It is equal to the plasmon absorption bandwidth Γ for the case of a perfectly free-electron gas in the limit $\gamma \ll \omega$ [23]. The damping constant γ is related to the lifetimes of all electron scattering processes which are mainly electron–electron, electron–phonon and electron–defect scattering in the bulk material [23]:

$$\gamma_0 = \sum_i \tau_i^{-1} = \tau_{e-e}^{-1} + \tau_{e-ph}^{-1} + \tau_{e-d}^{-1}, \tag{2.6}$$

where γ_0 is the bulk damping constant. As already mentioned above, for nanoparticles smaller than the mean free path of the conduction electrons, electron–surface scattering is believed to be important as well. An additional term accounting for electron–surface scattering is added to equation (2.6) and γ then becomes a function of the particle radius r as follows [74, 75]:

$$\gamma(r) = \gamma_0 + \frac{A\nu_F}{r}, \tag{2.7}$$

where A is a theory-dependent parameter which is dependent on the details of the scattering process (e.g. isotropic or diffuse scattering) [23, 63] and ν_F is the velocity of the electrons at the Fermi energy. This size effect is considered an intrinsic size effect [23] since the material dielectric function itself is size dependent, in contrast with the extrinsic size effect in large particles (i.e. $r > 20$ nm).

This model gives the correct $1/r$ dependence [46, 74, 75, 77, 78] of the plasmon bandwidth as a function of size for nanoparticles described by the dipole approximation in the intrinsic size region ($r < 20$ nm). The parameter A is mostly used as a fit parameter of the experimental results. However, the best advantage of this theory is probably the fact that it provides a very good description for the dependence of the particle dielectric constant on size. The modification of the dielectric constant is done in a straightforward manner. However, there exist many more theories [79–89] discussing how different factors such as the changes in the band structure, environmental changes or the 'spill-out' of the conduction electrons can be incorporated into a size-dependent dielectric function and thus into the main framework of the Mie theory. Other theories calculate the optical response from first principles by quantum-mechanical methods [87] or by the use of the jellium model for small clusters [88]. This is rather difficult to use by most synthetic or physical chemists trying to explain trends in the optical absorption spectra as a function of particle size. A compilation and comprehensive overview of these theories with references to the original work can be found in [23]. While all of them predict a $1/r$ dependence of the plasmon bandwidth, the calculated slope of this relationship covers a wide range of

values. More complicated is the prediction of the resonance absorption maximum as a function of particle size as many theories predict both a red shift and a blue shift with decreasing particle size [23, 63]. The fact that both trends are also observed experimentally makes it difficult to assign the origin of the band maximum shift with size.

A good comparison between different sizes can also be difficult since most preparation methods are only able to synthesize nanoparticles in a limited size range. The chemical reduction with sodium citrate for example is limited to sizes above 5 nm [33–35] while the thiolate-stabilized gold clusters produced by reduction with sodium borhydride are only stable for diameters below 5 nm [28, 32, 64, 65]. The monodispersity of each sample in comparison with the others is also important as inhomogeneous broadening can complicate size dependence studies. While one might think that a comparison between particles prepared by different methods should be possible as the same gold core is present in all the nanoparticles (the fcc crystal structure does not change with decreasing particle size), the capping ligands (matrix) around the particle surface can have a very important influence on the plasmon bandwidth and position [1, 4, 63, 67, 89, 90]. Henglein and co-workers [90] have shown that molecules adsorbed on silver nanoparticles will cause a pronounced broadening and damping of the surface plasmon resonance. One of the most recent theories that attempts to explain the size dependence of small nanoparticles in the intrinsic size range takes explicitly into account the chemical nature of the molecules capping the particles. Persson [89] developed a model known as the chemical interface damping (CID) model. In this model, the empty LUMOs of the acceptor molecules on the particle surface are coupled to the free electrons in the conduction band of the metal. The smaller the energy difference between the donor and acceptor levels, the stronger is the coupling. Electron transfer between the levels becomes possible after excitation of a plasmon resonance. Excited electrons transfer into the empty acceptor levels and then back. This causes their loss of coherence with the rest of the electrons excited during the plasmon excitation. This then corresponds to a broader bandwidth of the plasmon absorption. As the electronic structure (and therefore the energy position of the LUMO) varies for different adsorbate molecules, it is expected that the plasmon resonance of the same metal cluster will experience different degrees of damping depending on the specific adsorbed molecules. Kreibig and co-workers [67, 91] have shown experimentally how the plasmon band broadens when the same silver clusters produced in the gas phase are first deposited on a SiO_2 substrate and then later embedded in SiO_2 by co-deposition of SiO_2. In this unique experiment they were able to measure the surface plasmon absorption of 2 nm silver nanoparticles in the gas phase, deposited on a substrate and embedded in a matrix. The plasmon bandwidth increases as the clusters are surrounded by more SiO_2 molecules as expected from the model proposed by Persson [89]. They furthermore found very good quantitative agreement with the CID of the surface plasmon resonance. Therefore, it was proposed that the surface plasmon absorption could serve as a sensitive chemical sensor of the particle environment [92].

2.2. *Shape-dependent radiative properties: the Gans theory*

While size and environment (matrix) effects are very important, shape effects seem to be even more pronounced in the optical absorption spectrum of gold nanoparticles [44, 47, 53]. The plasmon resonance absorption band splits into two bands as the

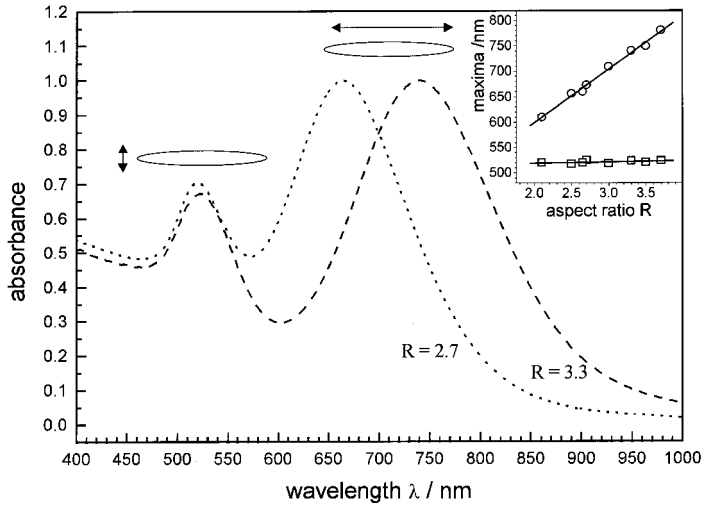

Figure 3. Size-dependent surface plasmon absorption of gold nanorods. Optical absorption spectra of gold nanorods with mean aspect ratios of 2·7 (· · · · ·) and 3·3 (– – –) are shown. The short-wavelength absorption band is due to the oscillation of the electrons perpendicular to the major axis of the nanorod while the long-wavelength band is caused by the oscillation along the major axis. The absorption bands are referred to as the transverse and longitudinal surface plasmon resonances respectively. The former is rather insensitive towards the nanorod aspect ratio in contrast with the longitudinal surface plasmon band which red shifts with increasing aspect ratio. This is illustrated in the inset where the two band maxima ((□), transverse mode; (○), longitudinal mode) are plotted against the nanorod aspect ratio *R*.

particles become more elongated along one axis [58–60]. The aspect ratio is the value of the long axis (length) divided by the short axis (width) of a cylindrical or rod-shaped particle. As the aspect ratio increases, the energy separation between the resonance frequencies of the two plasmon bands increases [58–60]. The high-energy band absorbing at around 520 nm corresponds to the oscillation of the electrons perpendicular to the major (long) rod axis and is referred to as the transverse plasmon absorption. This absorption band is relatively insensitive to the nanorod aspect ratio [44, 47, 53] and coincides spectrally with the surface plasmon oscillation of the nanodots. The other absorption band at lower energies is caused by the oscillation of the free electrons along the major (long) rod axis and is known as the longitudinal surface plasmon absorption. Figure 3 shows the absorption spectra of two nanorod samples having aspect ratios of 2·7 and 3·3. The samples were prepared electrochemically using micelles as the rod-shaping and stabilizing agents [44, 53]. Figure 3 shows that the longitudinal plasmon band maximum (open circles) red shifts with increasing aspect ratio while the transverse absorption band maximum (open squares) does not change [44, 47, 53, 93].

The optical absorption spectrum of a collection of randomly oriented gold nanorods with aspect ratio *R* can be modelled using an extension of the Mie theory. Within the dipole approximation according to the Gans [94] treatment, the extinction cross-section σ_{ext} for elongated ellipsoids is given by the following equation [58]:

$$\sigma_{ext} = \frac{\omega}{3c}\varepsilon_m^{3/2} V \sum_j \frac{(1/P_j^2)\,\varepsilon_2}{\{\varepsilon_1 + [(1-P_j)/P_j]\,\varepsilon_m\}^2 + \varepsilon_2^2}, \tag{2.8}$$

where P_j are the depolarization factors along the three axes A, B and C of the nanorod with $A > B = C$, defined as

$$P_A = \frac{1-e^2}{e^2}\left[\frac{1}{2e}\ln\left(\frac{1+e}{1-e}\right)-1\right], \tag{2.9}$$

$$P_B = P_C = \frac{1-P_A}{2}, \tag{2.10}$$

and the aspect ratio R is included in e as follows:

$$e = \left[1-\left(\frac{B}{A}\right)^2\right]^{1/2} = \left(1-\frac{1}{R^2}\right)^{1/2}. \tag{2.11}$$

2.3. *Effective dielectric function of a metal–host composite material: the Maxwell-Garnett theory*

In general, the Mie theory is only valid for very low concentrations of the nanoparticles in a solvent or solid matrix [23, 58]. It is assumed that the individual particles are non-interacting and separated from one another. Therefore, the electric field created around one particle by the excitation of a surface plasmon resonance is not felt by the other surrounding particles. If the interparticle distances become smaller than the particle dimension or if aggregation occurs, the plasmon resonance red shifts and often a second absorption peak at a longer wavelength is observed [23, 63, 95–97]. This band could be regarded as a longitudinal resonance absorption similar to the nanorods in the case of chain-like aggregation of the individual nanodots. In the case of particle aggregation and for composite materials such as densely packed nanoparticles in a transparent host medium, the effective-medium theories are better suited to explain their optical absorption spectra [23, 58, 63].

The Maxwell-Garnett [57] theory is an effective-medium theory. It treats the metal–dielectric composite material in which the particles are embedded and isolated from each other. The particle dimension and interparticle distances are considered to be infinitely small compared with the wavelength of the interacting light [58]. The Maxwell-Garnett theory is based on the Clausius–Masotti equation and it assumes that it is justified to describe the composite material containing metal nanoparticles embedded in an inert host medium by an effective complex dielectric constant ε_c such that [23, 48–51, 58, 98, 99]

$$\frac{\varepsilon_c-\varepsilon_m}{\varepsilon_c+\kappa\varepsilon_m} = f_m\frac{\varepsilon-\varepsilon_m}{\varepsilon+\kappa\varepsilon_m}, \tag{2.12}$$

where ε and ε_m are the dielectric constants of the metal nanoparticles and the host medium respectively. In contrast with the Mie theory, ε_m is also a complex function depending on the frequency of light. f_m is the volume fraction of the metal nanoparticles in the composite material and κ is a screening parameter. The latter is related to the shape of the nanoparticles [98, 99]. It has a value of two for spherical particles and equals one for long nanorods oriented with their axes of revolution parallel to the direction of the incident light. Its value approaches infinity for flat discs oriented with their axes of revolution perpendicular to the incident light [48–51]. With knowledge of ε and ε_m from the literature and an estimation of f_m from the sample preparation procedure, the dielectric constant ε_c of the composite material can be

computed with equation (2.12). The absorption spectrum of the metal nanoparticles in a transparent non-interacting host medium can then easily be calculated, as the dielectric constant is related to the optical refractive index n_c and the absorption coefficient k_c in the following way [58]:

$$\varepsilon_c = n_c^2 = \varepsilon_c' + i\varepsilon_c'', \tag{2.13a}$$

$$\varepsilon_c' = n_c^2 - k_c^2, \tag{2.13b}$$

$$\varepsilon_c'' = 2 n_c k_c. \tag{2.13c}$$

Martin and co-workers [48–52] have used an extended Maxwell-Garnett theory in order to explain the optical absorption spectra of needle-like and pancake-like gold nanoparticles in a porous alumina membrane. The particles are prepared by electrochemical deposition of the gold into the nanopores of the aluminium oxide template. The particles are all well aligned in one direction parallel to each other and the aspect ratio was controlled by the deposition time.

Palpant *et al.* [100] synthesized gold clusters in an alumina matrix in the size range 2–4 nm by laser vaporization of the metal and co-deposition with a dielectric vapour as a thin film on a substrate. The surface plasmon absorption of these small gold nanoparticles is strongly damped and blue shifts with decreasing particle size. They explained their experimental results by use of the Maxwell-Garnett theory and in combination with calculations based on the time-dependent local-density approximation [100].

3. Luminescence properties of metal nanoparticles

Photoluminescence from bulk copper and gold was first observed by Mooradian [101] and has been used extensively in characterizing the carrier relaxation and the band structure of metals [102–107]. It was found that the emission peak was centred near the interband absorption edge of the metal and therefore was attributed to direct radiative recombination of the excited electrons in the sp band with the holes in the d band [107]. However, the quantum efficiency of the photoluminescence from bulk noble metals is very low, typically of the order of 10^{-10} [101]. A theoretical model explaining the radiative recombination in noble metals was developed by Apell and Monreal [106]. Because of the slight overlap between the sp conduction band and the d band, the luminescence band shows a Stokes shift [107]. A more extensive experimental study on the photoluminescence of copper, silver and gold was carried out by Boyd *et al.* [103]. They were able to model their experimental results and determined the relation between the spectral peaks and the interband recombination transitions at selected symmetry points in the Brillouin zone.

Furthermore, Boyd *et al.* [103] studied the effect of the surface roughness on the photoluminescence properties of noble metals. The luminescence was found to be enhanced by several orders of magnitude on rough metal surfaces, which is known as the lightning rod effect [103, 108, 109]. The rough metal surface can be regarded as a collection of randomly oriented hemispheroids of nanometre size dimension on a smooth surface. These hemispheroids show a surface plasmon resonance and therefore the incoming and outgoing electric fields are amplified by the local field induced around the hemispheroids by the plasmon resonances [103, 108, 109].

The same local field effect is also observed in the Raman scattering from molecules absorbed on rough surfaces of noble metals, nanoparticle aggregates or single nanoparticles [15, 16, 110–118]. The surface-enhanced Raman scattering (SERS)

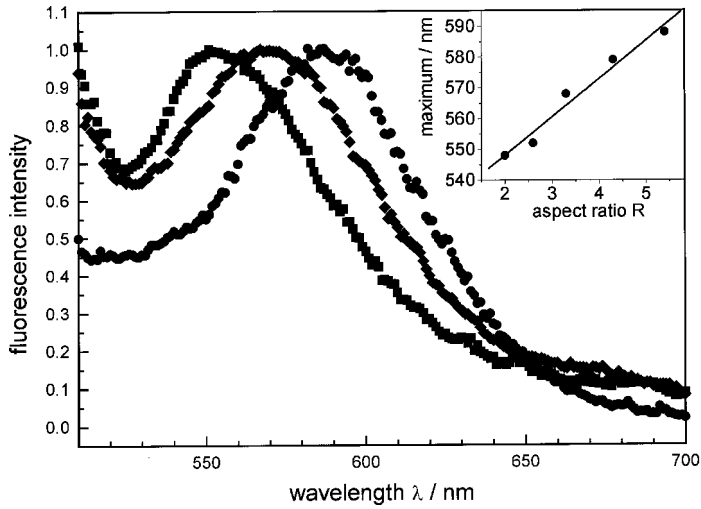

Figure 4. Size dependence of the luminescence properties of gold nanorods. The main plot shows fluorescence spectra of nanorods having mean aspect ratios of 2.6, 3.3 and 5.4. The fluorescence spectra are normalized at their respective maxima and the excitation wavelength was 480 nm. The fluorescence maximum red shifts with increasing aspect ratio R. This dependence is found to be linear as illustrated in the inset.

signal is enhanced by several orders of magnitude. While the chemical nature of the absorbed molecule and the bonding to the metal surface plays a role in SERS [110, 111] it is also recognized that an important component of the enhanced Raman scattering is due to the enhancement of the electromagnetic fields close to the nanoparticle surface [15, 16, 112, 113]. The nanoparticles can therefore be regarded as nano-amplifiers and, since the discovery of this effect, SERS spectroscopy has been studied intensively [15, 16, 110–118]. It is a convenient tool of increasing the sensitivity of an otherwise weak Raman signal.

A similar enhancement has recently been found by our group for the luminescence of gold nanorods [119]. The luminescence efficiency is increased by six orders of magnitude because of the lightning rod effect. Figure 4 shows the steady-state fluorescence spectra of three gold nanorod samples having average aspect ratios of 2.6, 3.3 and 5.4 after excitation at 480 nm. The spectra reveal the presence of an emission band between 550 and 600 nm. The fluorescence maximum red shifts with increasing nanorod aspect ratio. This is illustrated in the inset of figure 4 where the band maximum of the fluorescence emission is plotted against the nanorod aspect ratio. A linear dependence was found experimentally [119]. However, the luminescence quantum efficiency increases linearly with increasing square of the aspect ratio [119]. On the other hand, gold nanodots with diameters of between 10 and 30 nm prepared by the same electrochemical method do not show a comparable emission. This leads to the conclusion that the longitudinal plasmon resonance absorbing at a longer wavelength is more effective in amplifying the fluorescence intensity in gold nanoparticles than the surface plasmon resonance of spheres. This could be because the longitudinal plasmon resonance is less damped and has a much larger oscillator strength.

Wilcoxon *et al.* [120] reported that very small spherical gold clusters (less than 5 nm) show an emission at 440 nm when excited at 230 nm. The quantum yield is increased to 10^{-4}–10^{-5}, which is comparable with the enhancement of the photo-

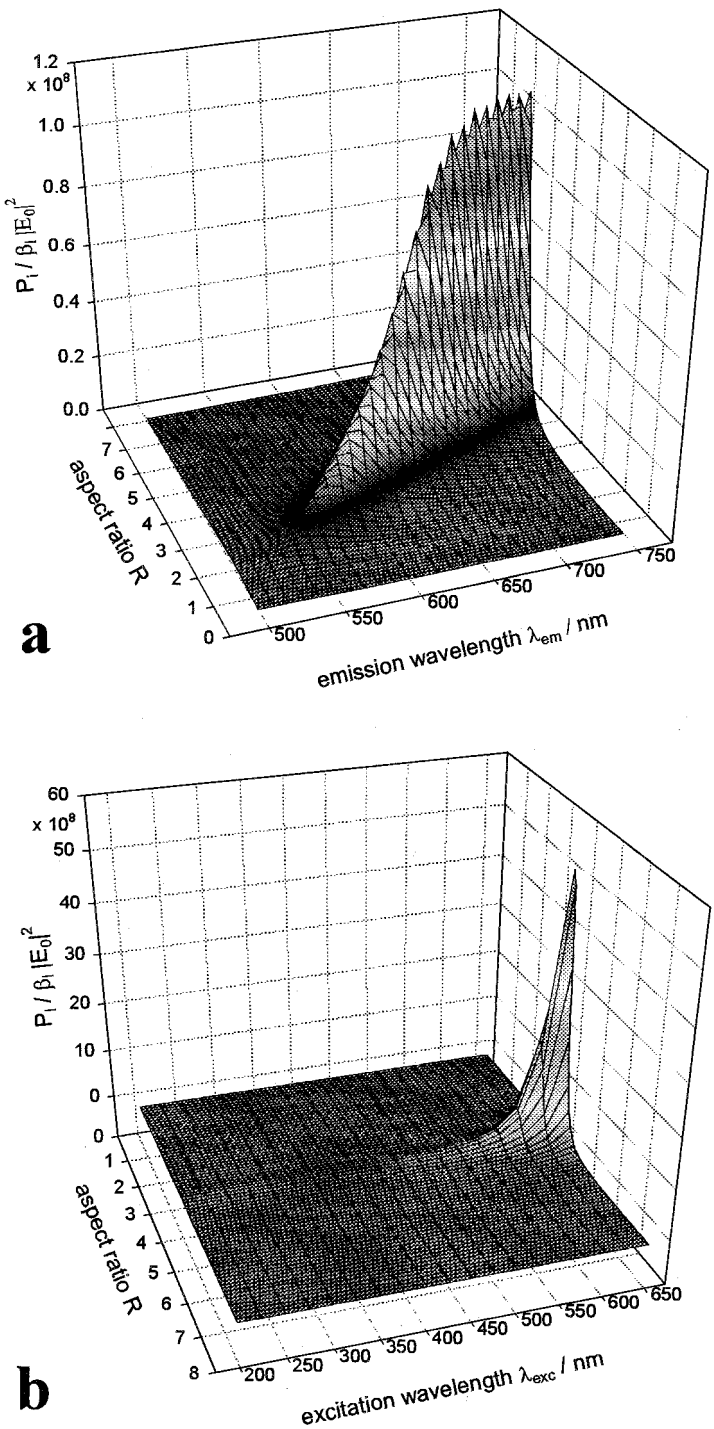

Figure 5. Theoretical modelling of the luminescence enhancement for gold nanorods with various aspect ratios. (*a*) The calculated single-photon luminescence power $P_l/|E_0|^2\beta_l$ emitted from gold nanorods as a function of the emission wavelength and the nanorod aspect ratio. The excitation wavelength was chosen to be 500 nm. (*b*) The calculated single-photon luminescence power $P_l/|E_0|^2\beta_l$ emitted from gold nanorods as a function of the excitation wavelength and the nanorod aspect ratio. The emission wavelength was chosen to be 650 nm.

luminescence of gold nanorods. These workers [120] showed that the luminescence is absent in larger nanodots of 15 nm diameter and concluded that the photoluminescent signal is affected by the capping ligands, such as thiols or amines.

In the above studies [119, 120] the origin of the photoluminescence was attributed to the radiative recombination of an electron–hole pair. The incident photons are initially absorbed by the d-band electrons, leading to interband transitions. The photon energy promotes these electrons from the filled d band to electronic states above the Fermi level in the sp conduction band. Even if the excitation is carried out in the plasmon band, rapid relaxation to the interband transition must take place. Electrons and holes relax by phonon scattering processes and some recombine radiatively to give rise to the observed luminescence. Such an intrinsic emission profile is, however, modified by the local field induced around the nanoparticles owing to excitation of the plasmon resonance. The theory of the local field effect has been successfully applied in various cases to explain results on second-harmonic generation [108], SERS [109] and luminescence [103] observed from rough noble metal surfaces. In order to test this mechanism for the photoluminescence enhancement in gold nanorods, we calculated the photoluminescence power of gold nanorods as a function of the emission wavelength and the nanorod aspect ratio [119]. According to the theoretical studies of the photoinduced luminescence [103] from rough surfaces of noble metals, the incoming and outgoing fields are proposed to be enhanced via coupling to the local plasmon resonances. The rough surface is assumed to be a random collection of non-interacting hemispheroids of height a and radius b. The volume is $V = \frac{4}{3}\pi ab^2$. The local field correction factor $L(\omega)$ within the spheroid is then given by [103, 109]

$$L(\omega) = \frac{L_{\mathrm{LR}}}{\varepsilon_1(\omega) + \mathrm{i}\,\varepsilon_2(\omega) - 1 + L_{\mathrm{LR}}\{(1 + \mathrm{i}4\pi^2 V)\,[1 - \varepsilon_1(\omega) - \mathrm{i}\,\varepsilon_2(\omega)]/3\lambda^3\}}, \tag{3.1}$$

where L_{LR}, called the lightning-rod factor, is defined as $L_{\mathrm{LR}} = 1/A$ where

$$A = \frac{1}{1 - \xi\, Q_1'(\xi)/Q_1(\xi)}, \quad \xi = \frac{1}{[1 - (b/a)^2]^{1/2}},$$
$$Q_1(\xi) = \frac{\xi}{2}\ln\left(\frac{\xi + 1}{\xi - 1}\right) - 1, \quad Q_1'(\xi) = \frac{\mathrm{d}Q_1(\xi)}{\mathrm{d}\xi}.$$

From equation (3.1) the single-photon luminescence power P_1 can be calculated [103] for excitation and emission energies $h\omega_{\mathrm{exc}}$ and $h\omega_{\mathrm{em}}$:

$$P_1 = \beta_1 2^4 |E_0|^2\, V |L^2(\omega_{\mathrm{exc}})\, L^2(\omega_{\mathrm{em}})|, \tag{3.2}$$

where β_1 is a constant that includes the intrinsic luminescence spectrum of the gold and E_0 is the incident electric field.

Assuming that the luminescence enhancement of the gold nanorods is due to the local field factor, $P_1/|E_0|^2\beta_1$ was calculated as a function of the gold nanorod aspect ratio and emission wavelength. The excitation wavelength was 500 nm. The results of these calculations [119] are shown in figure 5(*a*). The resonant luminescence power increases with increasing nanorod aspect ratio (lightning-rod effect) and shifts to longer emission wavelength. Furthermore, note that $P_1/|E_0|^2\beta_1$ is of the order of 10^7.

Both the red shift of the photoluminescence of the gold nanorods and the magnitude of the luminescence power due to the local field correction factor are in good agreement with the experimental results [119].

$P_l/|E_0|^2\beta_l$ was also calculated as a function of the excitation wavelength and the gold nanorod aspect ratio for a fixed volume. The emission wavelength was set at 650 nm. The results of this calculation are shown in figure 5(*b*) for the 200–650 nm excitation wavelength range. $P_l/|E_0|^2\beta_l$ is resonantly enhanced for an aspect ratio of about 4.5. This value of the aspect ratio depends critically on the chosen emission wavelength. Furthermore, the luminescence power greatly increases with increasing excitation wavelength.

From the calculation in figure 5, it follows that the luminescence power increases linearly with increasing square of the nanorod aspect ratio (or increasing square of the length for a fixed nanorod width) while a linear dependence on the aspect ratio is found for the wavelength of the emission maximum. These results are in good agreement with the experimental observations. This fact, therefore, strongly supports the assignment of the origin of the fluorescence from gold nanorods. This also suggests that the mechanism of the large enhancement in the luminescence efficiency is a result of the great enhancement of the field of the incoming exciting light and the outgoing emitted light via the coupling to the surface plasmon resonance.

4. Electron dynamics in gold nanoparticles probed by femtosecond transient absorption spectroscopy

4.1. *Introduction*

In order to study the interaction between the electrons and the lattice vibrations (phonons) in bulk materials, time-resolved transmission and reflectivity [121–132] as well as two-photon photoemission spectroscopies [133–138] have been used on thin films of metals and semiconductors. A better understanding of the thermal and electrical conductivity and also superconductivity was one of the goals of this research. With the advancement of ultrashort laser pulses, one can selectively excite the electrons of the metal and then follow the electron–phonon coupling in real time. It was suggested [121, 122] that this should in principle be possible with laser pulses shorter than the electron–phonon energy relaxation time. Because of the high electron density in metals, electron–electron interactions were expected to be strong enough to thermalize the electron gas within the duration of the exciting laser pulse. According to the two-temperature model (TTM) [139] the electrons and the lattice can be treated as two coupled subsystems. The separation of the electron gas and the lattice is justified because of the large difference in their heat capacities. The electrons absorb the photon energy, leading to a non-equilibrium temperature difference between the electron gas and the lattice directly after the laser pulse. Electron–phonon collisions then give rise to the excitation energy exchange between the electron subsystem and the lattice (energy relaxation T_1). In this manner a thermal equilibrium is reached. The time evolution of the electron and the lattice temperatures are expressed mathematically by the following two coupled differential equations within the TTM [139]:

$$C_e(T_e)\frac{\partial T_e}{\partial t} = -g(T_e - T_l) + \nabla \cdot (\kappa' \nabla T_e) + \mathrm{LP}(z, t), \tag{4.1}$$

$$C_l\frac{\partial T_l}{\partial t} = g(T_e - T_l), \tag{4.2}$$

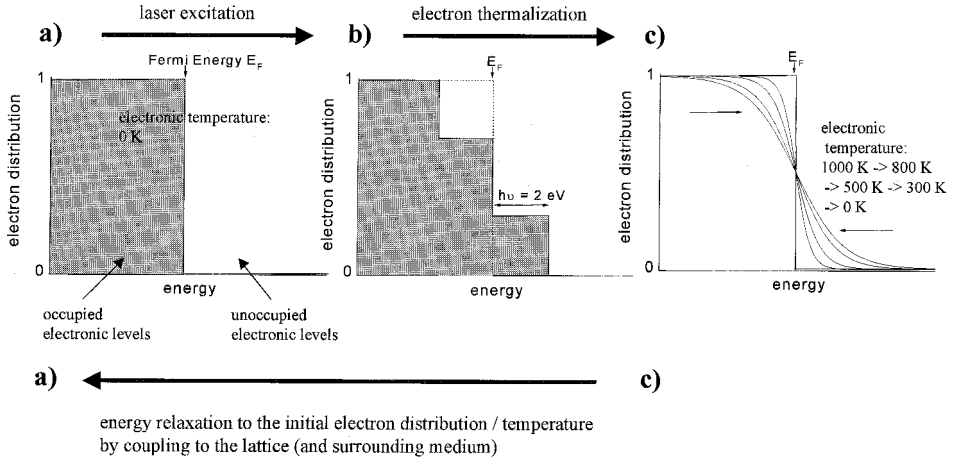

Figure 6. Schematic illustration of the electron distribution in the conduction band of a metal (nanoparticle). (*a*) Before laser excitation all states below the Fermi energy are occupied while all states above the Fermi energy are unoccupied. This would correspond to an initial temperature of 0 K, which was chosen for simplicity in this case. (*b*) Excitation with a laser pulse promotes electrons with energies of up to the excitation energy below the Fermi energy to states above the Fermi energy having a maximum energy equal to the excitation energy (2 eV or 620 nm in this illustration). This electron distribution is a non-thermal electron distribution with regard to Fermi–Dirac statistics, which describes the electron distribution for a given electron temperature. This non-thermal electron distribution relaxes (thermalizes) by electron–electron scattering without losing the absorbed photon energy. (*c*) In this case an electron temperature of 1000 K is reached. (Energy conservation requires that the areas under the curves in (*b*) and (*c*) for energies greater than the Fermi energy have to be equal.) Electron–phonon coupling and phonon–phonon interactions with the surrounding medium lead to the cooling of the electron gas as illustrated by the other curves in (*c*). Finally, the system returns to its starting electron temperature (*a*).

where C_e and C_l are the electronic and lattice heat capacities respectively, g is the electron–phonon coupling constant and κ' is the electronic thermal conductivity describing the heat transport away from the excited laser spot (which can be neglected in case of the nanoparticles as they are smaller than the excitation spot). $LP(z, t)$ is the spatial and temporal evolution of the exiting laser pulse. The electronic heat capacity $C_e(T_e)$ is usually assumed to vary linearly with the electron temperature T_e.

Although pump–probe laser spectroscopy measures the optical (transient absorption, transmission or reflectivity) rather than thermal response of an excited sample, it is justified in the case of metal films to express the changes induced by the pump pulse in terms of temperature changes. This idea might be strange for a molecular spectroscopist following the excitation of a single electron between two electronic levels, but the reason for this argumentation is that the metal film can absorb several photons. The appropriate way to describe a new electron distribution within the conduction band of the metal is by Fermi–Dirac statistics [76] (after a rapid internal electron relaxation by elastic electron–electron collisions has taken place). Each Fermi electron distribution is associated with an electronic temperature. Therefore, the energy relaxation of the electron gas into the lattice motion is best followed by its electronic temperature.

The scheme in figure 6 illustrates the changes in the electronic energy distribution within the conduction band of the metal after laser excitation. For simplicity, only

intraband excitations are considered in this picture. Furthermore, it is assumed that the experiment is carried out at an initial temperature of 0 K. The electron distribution f shown in figure 6(*a*) is calculated according to the Fermi–Dirac statistics and has the mathematical form [76]

$$f = \frac{1}{1+\exp(E-E_F/kT)}, \tag{4.3}$$

where k, T, E_F and E are the Boltzmann constant, the temperature, the Fermi energy and the energy of the electronic energy levels respectively.

Excitation with a wavelength of 620 nm corresponds to a photon energy of 2.0 eV. This excites electrons having an energy of less than or equal to 2.0 eV below the Fermi level to electronic levels up to 2 eV above the Fermi level. The corresponding electron distribution is plotted in figure 6(*b*). This electron distribution is not the equilibrium distribution according to the occupation dictated by the Fermi–Dirac statistics for fermions. Electron–electron scattering within the electron gas occurs until a new Fermi electron distribution with a higher electron temperature is reached as illustrated in figure 6(*c*). This leads to an internal electron thermalization [127, 128]. Electron–electron interactions are elastic and the overall energy is conserved during this first relaxation process. External thermalization [127, 128] with the phonon bath will then initially lead to a temperature equilibration between the electron and the lattice subsystems. As the excited electrons above the Fermi level now lose their energy to the phonons, the Fermi distribution narrows until a situation shown in figure 6(*a*) is reached, assuming that there is also heat release to the surrounding system. During the external thermalization the temperature of the electron gas (and the lattice) decreases steadily and the whole system returns to its original (ground) state prior to laser excitation.

Interband transitions lead to a very similar picture especially if one remembers that recombination of the holes in the low-lying d band with any of the excited electrons above the Fermi level or the unexcited electrons below the Fermi level occurs on the tens of femtoseconds time scale [140–142], that is faster than or comparable with the duration of the exciting laser pulse. It is the high density of the charge carriers in the conduction band that leads to fast interband relaxation. If one assumes for the interband relaxation that an Auger-type recombination mechanism process takes place, then highly excited electrons are present within the conduction shortly after the excitation pulse. These electrons have an average excess energy above the Fermi level equal to the exciting photon energy as the holes in the d band have already been filled by the initial electron–electron scattering. Although interband transitions might therefore complicate the initial relaxation dynamics, they should not change the overall picture.

Typical electron–phonon relaxation times of the order of a few picoseconds were measured for thin gold films by time-resolved transmissivity and reflectivity [121–132] as well as two-photon photoemission spectroscopy [133–138] using femtosecond laser pulses. By measuring the transient optical response of metal nanoparticles, the effect of size on the electron–phonon coupling can directly be analysed. The reduction in the size and dimensionality of the material introduces new boundaries as in the nanoparticle surfaces. Enhanced electron–surface scattering [74, 75] was already discussed as a mechanism for the dephasing of the coherent plasmon oscillation and could also be important for the energy relaxation of hot electrons. The reduction in the density of electron and phonon states could further alter the relaxation dynamics in

these zero-dimensional dots. However, in the size range of gold nanoparticles discussed so far (10–100 nm), the bulk gold band structure of the nanoparticles is expected to be well developed. The average energy spacing between adjacent energy levels within the conduction band is small compared with the thermal energy. Quantum size effects in the relaxation dynamics are therefore expected to occur only in very small gold clusters which lack an intense plasmon absorption. The presence of a well developed plasmon band can, however, be very advantageous in following the optical response of excited metal nanoparticles as has been shown in many studies [143–167]. Furthermore, for about 200 000 atoms in a 20 nm gold nanoparticle, and hence with many conduction electrons, the same general theory (many-electron excitation described by an effective electron temperature) as applied for metal films [121–138] can be used. This especially holds because of the large extinction coefficients of the gold nanoparticles. Experimentally, a transient broadening of the surface plasmon absorption is observed which results in a bleach at the plasmon absorption band maximum with two positive absorption features at higher and lower energies. The rate of the bleach recovery directly monitors the rate of the electron–electron, electron–phonon and phonon–phonon dynamics, which will be illustrated in more detail below.

4.2. *Theoretical modelling of the transient optical response*

Theoretically, the broadening of the plasmon band can be related to the changes in the real and imaginary parts of the complex dielectric function [124, 127, 128, 147, 165, 166]. Changes in ε_1 and ε_2 will affect the plasmon absorption as can be shown from equation (2.3). The changes in the real and imaginary parts of the dielectric function can be related to the changes in the electron distribution function as suggested in a model developed by Rosei *et al.* [168, 169] for continuous-wave thermomodulation experiments. Using the constant-matrix approximation, the change in the imaginary part of the dielectric function is given by [128]

$$\Delta\varepsilon_2 \propto \frac{1}{(h\nu)^2}\int D(E, h\nu)\,\Delta\rho\,\mathrm{d}E, \tag{4.4}$$

where $D(E, h\nu)$ is the joint density of states with respect to the energy E of the final state and $\Delta\rho$ denotes the change in the electron distribution f as given by equation (4.3). $D(E, h\nu)$ is calculated assuming parabolic band structures for the d band and conduction band in the vicinity of the L point of the Brillouin zone [168]. This determines $\Delta\varepsilon_2$ for a given change $\Delta\rho$ in the electron distribution. The change $\Delta\rho$ in the electron distribution for a thermalized electron gas is calculated from the difference between the two Fermi electron distributions at room temperature and at a higher temperature corresponding to a certain laser excitation. The change $\Delta\varepsilon_1$ in the real part of the dielectric constant is then computed from $\Delta\varepsilon_2$ using the Kramers–Kronig relationship [76]:

$$\Delta\varepsilon_1(h\nu) = \frac{2}{\pi}P\left(\int \frac{h\nu'\,\Delta\varepsilon_2(h\nu')}{(h\nu')^2 - (h\nu)^2}\mathrm{d}(h\nu')\right), \tag{4.5}$$

where P denotes a Cauchy principal value integral which extends over the whole frequency range.

The differential transmission $\Delta T/T$ of the gold nanoparticles at low excitation levels is approximately equal to the change in absorption and can be expressed as

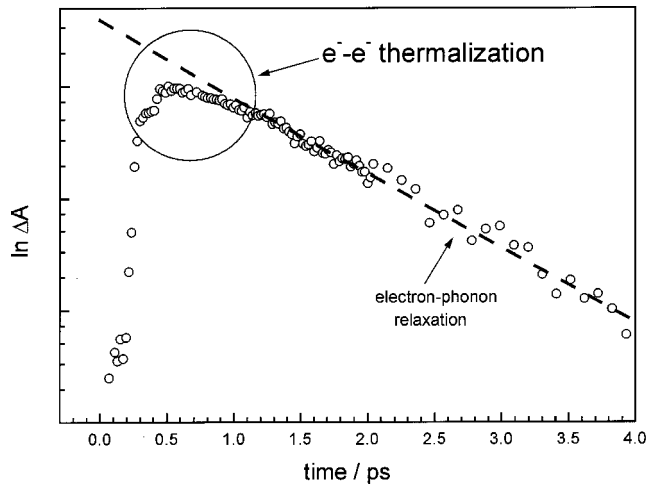

Figure 7. Electron–electron thermalization in spherical gold nanoparticles. The plasmon bleach recovery of 22 nm gold nanoparticles probed at 530 nm is plotted against a logarithmic scale. The excitation wavelength was 800 nm, therefore exciting only intraband transitions. The broken line corresponds to a fit with a lifetime of 1·7 ps. The recorded signal, however, shows a distinct deviation from a pure single-exponential behaviour at early delay times which was attributed to a finite electron–electron thermalization. (Note that this kinetic trace was originally a transient bleach signal before applying the natural logarithm.)

linear combinations of the induced changes $\Delta\varepsilon_1$ and $\Delta\varepsilon_2$ in the real and imaginary parts respectively of the dielectric constant [128]:

$$\frac{\Delta T}{T} = \frac{\delta(\ln T)}{\delta\varepsilon_1}\Delta\varepsilon_1 + \frac{\delta(\ln T)}{\delta\varepsilon_2}\Delta\varepsilon_2. \tag{4.6}$$

The coefficients of proportionality can be calculated using the theoretical expression for the plasmon band absorption as given by equation (2.3). This model has been used successfully describing the optical response of metal nanoparticles excited by an ultrashort laser pulse [147, 165, 166].

4.3. *Electron–electron thermalization in gold nanoparticles*

Figure 7 shows a kinetic trace recorded at 530 nm after excitation with 800 nm femtosecond laser pulses [166]. The signal intensity is plotted on a logarithmic scale. A single-exponential decay, neglecting the long-time component due to phonon–phonon interactions, should give a straight line. However, deviations from a linear dependence at early times are clearly visible. In fact, the signal is not as intense as would be expected from a purely single-exponential decay. This observation can be related to the non-thermal electron distribution [129]. Calculation of the transient absorption spectrum using the formalism and equations outlined above showed that the bleaching of the plasmon band is less intense for a non-thermal than for a thermalized electron distribution [128, 166]. Basically, one observes a delayed rise in the signal intensity corresponding to the internal thermalization of the electron gas. Using a rate equation model derived by Sun *et al.* [128] for their measurements on thin gold films, an electron thermalization time of 500 fs is obtained for the experimental results shown in figure 7 [166]. This relaxation time equals the time that it takes for all the electrons to scatter with each other in such a way that a Fermi distribution is

reached. This is of course longer than a scattering event involving only two electrons, which is of the order of 10 fs according to the Fermi-liquid theory [170]. The reason why the effect of these processes on the transient absorption is rather small (compared with theoretical results) and why it is only detectable at low pump powers [166] is the fact that processes outlined in figure 6 (electron–electron, electron–phonon and phonon–phonon scattering) are not really sequential processes. Electron–phonon coupling will relax the hot initial electron distribution before an equilibrium Fermi electron distribution can be fully established. This is, however, taken into account in the rate equation with which a thermalization time of 500 fs was calculated [128, 166].

4.4. *Electron–phonon relaxation in gold nanoparticles*

Figure 8(*a*) shows the transient absorption spectra of 15 nm gold particles at different delay times after the excitation pulse [166]. The excitation wavelength used for these studies was 400 nm and was produced by second-harmonic generation using the fundamental of an amplified titanium : sapphire laser system [166]. The transient absorption spectra are obtained by using a white-light continuum laser pulse with and without pulsed excitation at different delay times. The difference spectrum between the absorption of the gold nanoparticles after excitation and their 'ground-state' (unexcited) absorption is then calculated as a function of time. The plasmon band bleaches at its maximum, corresponding to a higher transmission of light of the excited solution. Two weaker absorption bands are also visible at lower and higher energies than the plasmon band maximum [143–145, 164–166]. These spectral features are due to a broadening of the surface plasmon resonance at higher electronic temperatures. Compared with the ground-state absorption, a broader but less intense plasmon absorption at a higher electronic temperature after laser excitation results in a bleach and two positive absorptions in the transient spectrum (difference spectrum). The fact that the important parameter is the electronic temperature explains the observation that the optical response is independent of the excitation wavelength [166]. At 400 nm or shorter wavelengths than the plasmon absorption, interband transitions from the d band to above the Fermi level are excited. Excitation at the plasmon resonance will cause the oscillation of the conduction electrons and basically results in the collective excitation of all the conduction electrons. This could be regarded as intraband transitions, which are also excited to the red of the plasmon band. (In gold nanoparticles of the size under study, the onset for intraband transition coincides with the plasmon maximum at about 2·4 eV [171]). All these excitation processes result in heating of the electron gas [166].

The laser-induced optical changes decay as the electronic temperature decreases and thermal equilibration between the electrons and the lattice is established [144, 147, 164]. The absorbed laser energy is then released to the surrounding medium by phonon–phonon interactions [144, 147, 164]. Measuring the bleach recovery as a function of time gives the electron–phonon and phonon–phonon relaxation times. Figure 8(*b*) shows such a kinetic trace. The observation wavelength is 520 nm, coinciding with the plasmon band bleach maximum where the transient signal is most sensitive. The data in figure 8(*b*) [166] were obtained from the transient absorption spectra recorded with a charge-coupled device camera by extracting the time dependence at a certain wavelength from the measured spectra. The plasmon bleach recovery can be fitted to a biexponential decay function giving relaxation times of 3·4 and about 100 ps. The first component corresponds to the electron–phonon interactions [164] while the long-time component is the energy relaxation (phonon–

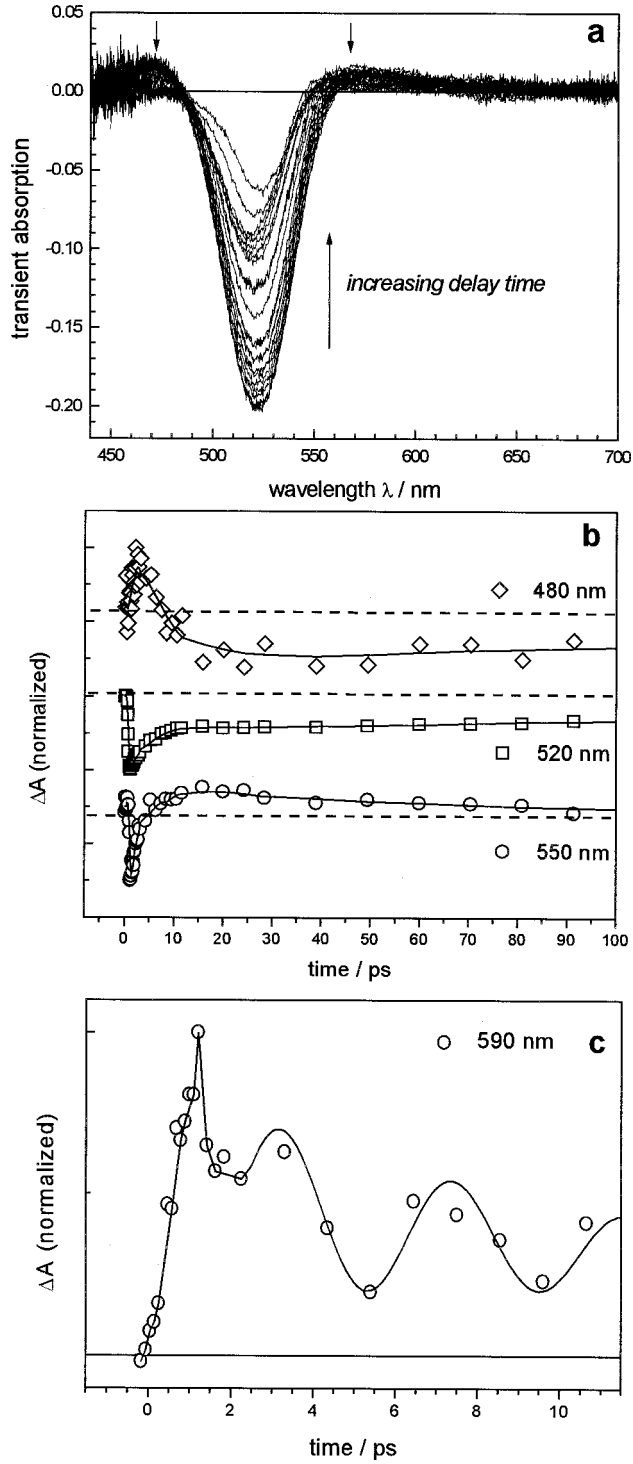

Figure 8. Optical response of spherical gold nanoparticles after excitation with a femtosecond laser pulse. (*a*) The transient absorption spectra of 15 nm gold nanoparticles after excitation with 400 nm laser light. The series of spectra corresponds to different delay times between the pump and probe pulses. The plasmon band is bleached (negative

phonon interactions [164]) of the hot lattice to the surrounding medium. The latter finally leads to complete cooling of the whole nanoparticle. Kinetic traces for other wavelengths are also shown in figure 8(*b*). At 480 nm the signal first shows absorption and then bleaches at later times. This can be explained by a red shift of the plasmon resonance [147] due to a volume expansion of the hot particles and hence a lower electron density and lower plasmon frequency (see section 2). Correspondingly, the transient absorption signal at 550 nm changes from a bleach into an absorption at a comparable time delay of about 10 ps. However, the change in the absorption signal at 550 nm not only could result from a red shift but also could be due to the narrowing of the plasmon bleach as the Fermi electron distribution cools.

A closer look at the kinetic traces at a longer wavelength than the plasmon band maximum reveals that the transient absorption signal oscillates with a period of about 5 ps (figure 8(*c*)). Del Fatti *et al*. [157, 158] and also Hartland and co-workers [148, 149] have shown that these quantum beats are indeed real and result from the low-frequency acoustic breathing modes of the hot nanoparticles. The acoustic breathing modes are impulsively excited by the rapid heating of the particle lattice after laser excitation [148, 149, 157, 158]. The volume of the nanoparticles increases and decreases periodically owing to the excitation of these modes. This in turn leads to a shift in the plasmon band maximum as the free-electron density changes with the volume. A volume expansion causes a drop in the free-electron density and a red shift of the plasmon, which is associated with an increase in the plasmon bleach intensity at low energies. At high energies, the acoustic breathing causes an oscillation of the transient absorption which is 180° out of phase with respect to the signal observed at low energies [158]. It was further found that the frequencies of the acoustic modes are inversely proportional to the nanoparticle radius [148, 149, 157, 158].

Physically, this transient behaviour of the plasmon band broadening is also associated with a faster dephasing time T_2 of the coherent plasmon oscillation [143–145]. At higher temperatures the occupation of higher electronic states leads to an increased electron scattering rate as known from the Fermi-liquid theory [170] and thus to an increased damping of the plasmon oscillation. Perner *et al*. [144] found an increase in the plasmon bandwidth of gold nanoparticles embedded in a sol–gel matrix by 120 meV and calculated an average electron–electron scattering rate of $(10\ \text{fs})^{-1}$ for a hot electron distribution at 4000 K. The decay of the transient plasmon band broadening follows the same kinetics as the decay of the bleach intensity. This is illustrated in figure 9 for 15 nm gold nanoparticles. The spectra are fitted to a Lorentzian line shape. The left inset in figure 8 shows the linewidth decay while the

---

absorption) and two positive absorption bands are visible at higher and lower energies as indicated by the arrows. The transient signal is due to a broadening of the plasmon resonance at higher electronic temperatures. (*b*) The temporal evolution of the recorded spectra at certain wavelengths ((◇), 480 nm; (□), 520 nm; (○), 550 nm). The signal recovers by electron–phonon coupling and phonon–phonon relaxation with molecules in the surrounding medium. These two processes are of the order of 1–4 and 100 ps respectively. (*c*) The temporal evolution of the transient absorption signal at 590 nm is shown on a shorter time scale. The oscillation is due to the low-frequency acoustic breathing modes of the host nanoparticles. These modes are impulsively excited by the rapid heating of the particle lattice and correspond to an oscillatory change in the volume of the hot nanoparticles. The line in (*c*) is not a fit to the data points but serves as a visual aid showing the beat signal. All kinetic traces in this figure were obtained directly from the measured transient absorption spectra in (*a*).

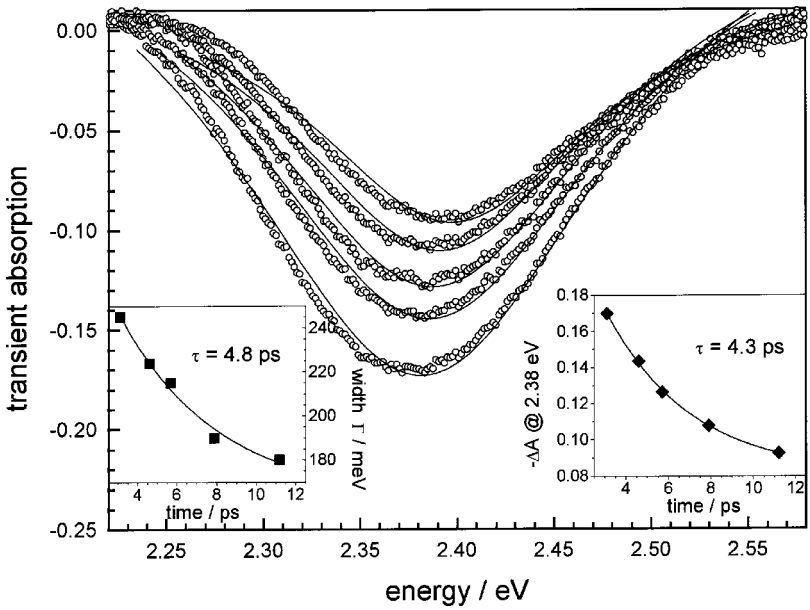

Figure 9. Transient absorption spectra of 15 nm gold nanoparticles after excitation at 400 nm with 100 fs laser pulses recorded at different delay times plotted against an energy scale (same spectra as shown in figure 8(*a*)). The left inset shows the decrease in the bleach linewidth with increasing delay time. The linewidth was obtained by fitting a Lorentzian function (———) to the experimental spectra (○). The right inset illustrates the decay of the transient bleach signal monitored at 2·38 eV. Exponential fits to the data points in the insets give similar decay times of 4·8 and 4·3 ps for the decay of the transient broadening and bleach intensity respectively.

right inset displays the decay of the plasmon bleach intensity at its maximum (2·38 eV). An exponential fit to the data points gives comparable lifetimes of 4·8 and 4·3 ps for the decay of the plasmon bleach linewidth and intensity respectively.

4.5. *Pump power dependence of the electron–phonon relaxation rate*

When discussing the measured electron–phonon relaxation times quantitatively, it is very important to note that the measured relaxation times are pump power dependent [146, 147, 165, 166]. As the electronic heat capacity depends on the electron temperature ($C_e \propto T_e$ [76]), the effective rate constant $g/C_e(T_e)$ of the thermal relaxation of the electron gas $\delta C_e/\delta T_e$ in equation (4.1) becomes temperature dependent. As a consequence, the experimentally measured electron–phonon relaxation time increases with increasing electron temperature and hence with increasing pump power [146, 147, 165, 166]. This is illustrated in figure 10, which shows the plasmon bleach recovery of 15 nm spherical gold nanoparticles at four different laser pump intensities. The monitoring and excitation wavelengths are 520 and 400 nm respectively [166]. The measured lifetimes increase from 1·5 to 3·6 ps. From a plot of the measured electron–phonon relaxation times versus power, the electron–phonon coupling constant can be obtained [146, 147] which compares well with the value measured for bulk gold films [124].

While the effects of the surrounding medium on the electron–phonon interaction cannot be excluded, the power dependence of the electron–phonon relaxation could also explain the slightly different results obtained for gold nanoparticles in solution or

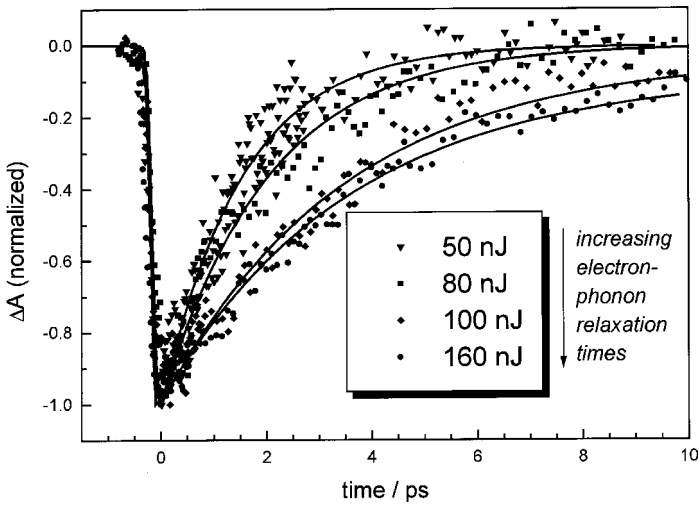

Figure 10. Pump power dependence of the electron–phonon relaxation time in gold nanoparticles. The plasmon bleach recovery of 15 nm gold nanoparticles is probed at 520 nm after excitation at 400 nm with laser pulses of various energies. The electron–phonon relaxation time increases with increasing laser pump power, since the electron heat capacity is temperature dependent.

embedded in a solid matrix by several researchers. Ahmadi *et al.* [164] reported decay times of 2·5 and more than 50 ps for the electron–phonon and phonon–phonon relaxation times in 30 nm colloidal gold particles. Inouye *et al.* [161] measured gold nanoparticles with a diameter of 7·6 nm in a SiO_2 glass matrix. They found decay times of 2·8 and 120 ps. Perner *et al.* [144] measured relaxation times of 4 and 200 ps for 30 nm gold particles embedded in a sol–gel matrix after excitation at 400 nm. Smith and co-workers [153–155], on the other hand, observed longer relaxation times of 7 and 400 ps for 15 nm gold nanoparticles in water. The monitoring wavelength was 790 nm with excitation at 390 nm, but the laser pulses had a much higher energy (several microjoules). The relaxation dynamics of the excited electrons in a nanoshell of gold sulphide nanoparticles coated with an outer layer of gold were reported by Averitt *et al.* [163] who found a lifetime of 1·7 ps, similar to the results on the pure gold nanoparticles.

Femtosecond studies have been carried out on other metal nanoparticles, in particular silver and copper. Hodak *et al.* [147] found lifetimes of about 1 ps for 10 and 50 nm silver particles. Roberti *et al.* [152] investigated 10 nm silver particles and found decay times of 2 and 40 ps when probed between 660 and 790 nm. A decay time of 0·7 ps was obtained for 4 nm copper nanoparticles in a glass matrix by Tokizaki *et al.* [162].

4.6. *Shape and size dependences of the electron–phonon relaxation rate*

When a gold nanorod sample is exposed to femtosecond laser pulses, both plasmon bands are bleached owing to a hot electron gas [167]. This is shown in figure 11 where the transient absorption (solid curve) and steady-state absorption (broken curve) spectra of gold nanorods with a mean aspect ratio of 3·8 are displayed. The transient absorption spectrum was recorded at a delay time of 6 ps after excitation with 100 fs laser pulses having a centre wavelength of 400 nm [167]. The bleach of the two bands

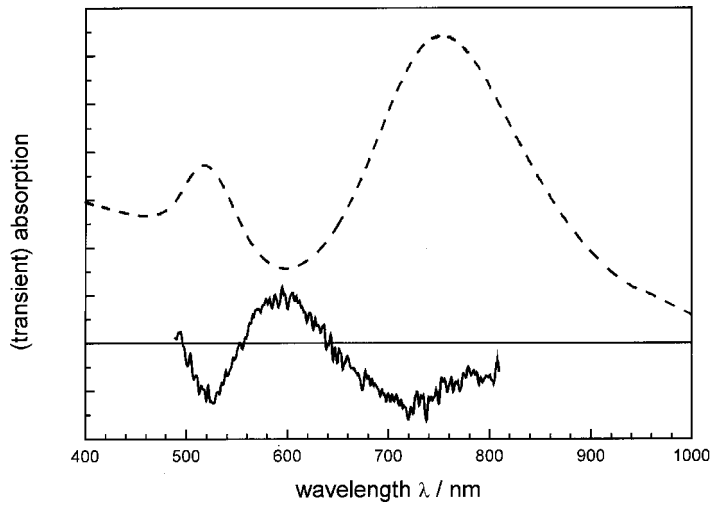

Figure 11. Optical response of gold nanorods after excitation with a femtosecond laser pulse. Transient absorption (———) and steady-state absorption spectrum (– – –) of gold nanorods with a mean aspect ratio of 3·8 are shown. Both spectra are scaled to arbitrary units. The transient absorption spectrum was recorded at a delay time of 6 ps after excitation with 100 fs laser pulses having a centre wavelength of 400 nm. The bleach of the two bands and the positive absorption around 600 nm are consistent with a broadening of the transverse and longitudinal surface plasmon bands due to a higher electronic temperature.

and the positive absorption around 600 nm are consistent with a broadening of the transverse and longitudinal surface plasmon bands. The transient absorption spectrum in figure 11 also suggests that the magnitude of the bleach is less pronounced for the longitudinal plasmon band than for the transverse. This is concluded from the intensity ratio of the two bands in the transient absorption spectrum compared with that for the steady-state spectrum. This last observation could, however, be somewhat obscured by the photothermal instability of the gold nanorods (see section 5 below).

One of the initial goals in studying the electron–phonon relaxation dynamics was the question of how the electron dynamics might change with particle size and shape. Since increased electron–surface scattering was thought to be responsible for the plasmon band broadening in the intrinsic size region, femtosecond transient absorption experiments are carried out to determine whether electron–surface collisions are mainly inelastic and, therefore, contribute effectively to energy relaxation. With a mean free path of about 40–50 nm in gold and silver [76], the measured electron–phonon relaxation time should increase with decreasing particle radius if the electron–surface scattering becomes an important relaxation pathway for small particles. The results of such an experiment are shown in figure 12. The plasmon bleach recovery measured for 48 and 15 nm gold nanoparticles is compared with the bleach recovery of the transverse and longitudinal modes of gold nanorods with an average aspect ratio of 3·8 (top to bottom). The laser pump power and optical densities of the samples at the excitation wavelength were adjusted so that comparable initial electron temperatures were induced by the exciting femtosecond laser pulse. This ensures that the measured relaxation times can be directly compared with each other. No significant change in the electron–phonon relaxation dynamics can be observed for 48 and 15 nm gold nanoparticles [166]. Furthermore, the relaxation dynamics appear

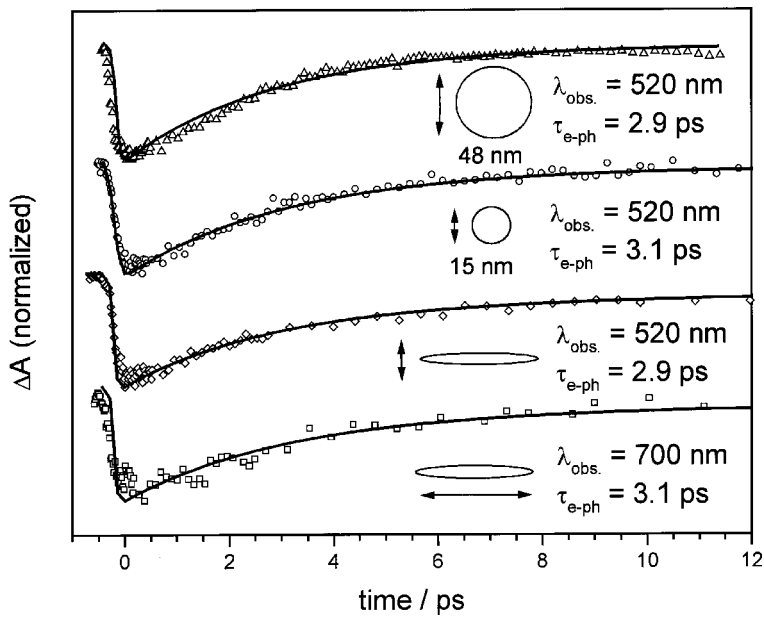

Figure 12. Size and shape dependences of the electron–phonon relaxation time. Plasmon bleach recovery measured for 48 and 15 nm gold nanoparticles and for the transverse and longitudinal modes of gold nanorods with an average aspect ratio of 3·8 (from top to bottom). The laser pump power and optical densities of the samples at the excitation wavelength were adjusted so that comparable initial electron temperatures were induced by the exciting femtosecond laser pulse. The results show that the measured electron–phonon relaxation times are independent of particle size and shape, eliminating the influence of electron–surface scattering as a dominant energy relaxation pathway.

to be independent of the particle shape and the specific plasmon band mode (transverse or longitudinal) as also shown in figure 12 [167]. In summary, these experimental results show that the measured electron–phonon relaxation times are independent of particle size and shape for gold in the investigated size range, eliminating the influence of electron–surface scattering as a dominant energy relaxation pathway.

Ahmadi *et al.* [165] also observed no size dependence of the electron–phonon relaxation for 1·9, 2·6 and 3·2 nm thiol-passivated gold nanocrystals which were compared with the measured relaxation dynamics of 30 nm colloidal gold nanoparticles prepared by the citrate method. The spectral changes in the transient absorption signal were attributed to a lower density of electronic states in the very small molecular-like nanoparticles. In agreement with these results, Hodak *et al.* [149] reported that the electron–phonon coupling constant (and hence the electron–phonon relaxation time) is independent of particle size for gold nanoparticles in the size range between 4 and 120 nm. They also found no change in the electron dynamics measured in 10 and 50 nm silver particles [147]. Hamanaka *et al.* [156] reported that the electron–phonon coupling constant and the electronic and lattice specific heats are size independent for silver nanocrystals with a diameter of more than 6 nm. They observed a decay of the plasmon band broadening with relaxation times of 2–3 and 200 ps. On the other hand, Stella *et al.* [172, 173] reported a size-dependent electron–surface interaction for 2, 4 and 6 nm tin particles embedded in an Al_2O_3 matrix by femtosecond transient reflectivity measurements. They measured decreasing lifetimes with

decreasing size, corresponding to an increase in electron–surface scattering in the tin nanoparticles where the mean free path is 4.4 nm. The same workers also obtained a size dependence of the hot electron relaxation time for solid and liquid gallium nanoparticles, which had mean diameters of 5, 7 and 9 nm [174]. Del Fatti *et al.* [159] reported a decrease in the electron–phonon relaxation times from 800 to 500 fs for silver nanoparticles in a glass matrix as the size is reduced from 30 nm to below 8 nm. This size dependence of the electron–phonon relaxation was also attributed to an enhanced inelastic electron–surface scattering. Smith *et al.* [155] compared 15 nm gold nanoparticles with Au_{13} and Au_{55} clusters. They also found a size dependence and proposed a model in which the relaxation dynamics of the photoexcited electron gas are described by two competing processes. Electron–phonon coupling decreases and electron–surface scattering increases with decreasing particle size. As the two processes compete with each other, they determine the measured lifetime.

In recent work, Hodak *et al.* [175] were able to explain the difference in the size dependence of the electron–phonon relaxation in different metallic nanoparticles. Based on a quantum kinetic treatment of the electron–surface coupling developed by Belotskii *et al.* [176, 177], they calculated the contribution of the electron–surface coupling constant to the total (bulk) coupling constant. They found that the excitation of capillary and acoustic surface modes by the scattering of the electrons with the particle surface accounts for less than 10% of the electron energy loss in gold nanoparticles as small as 2.6 nm. However, the relative magnitude of the electron–surface coupling constant compared with the total electron–phonon coupling constant depends on the ratio of the electron density to the metal density and therefore on the specific metal. The excitation of surface vibrations is suppressed in nanoparticles consisting of heavy atoms such as gold as the electrons scatter rather elastically. In nanoparticles made of lighter atoms with more valence electrons contributing to the conduction band, a size-dependent energy relaxation becomes possible via electron–surface interactions [175]. Using the same model, Nisoli *et al.* [174] were able to account completely for the size dependence of the electron–phonon relaxation in gallium nanoparticles, which consist of lighter atoms and a higher electron density.

5. Photothermal laser-induced shape transformation of gold nanoparticles

Electron–phonon coupling leads to thermal equilibration between the electrons and the lattice after selective excitation of the electron gas with a laser pulse as already discussed in detail in section 4. It was also mentioned that electron temperatures of several thousand kelvins are easily reached even with excitation powers as low as 100 nJ or typical fluences on the order of 1 mJ cm^{-2} corresponding to a tightly focused beam with a spot size of about 100–200 μm [144, 166]. Because of the difference in heat capacities [76] the change in the lattice temperature is only on the order of a few tens of degrees. This is no longer the case when the energy of the excitation pulse is increased to several microjoules (with no change in the spot size). The temperature of the nanoparticle lattice can then reach the melting temperature of the respective material. In several cases, size [178–181] and shape [182–185] changes have been observed for nanoparticles heated by laser exposure in colloidal solutions as well as in a solid glass matrix. Usually TEM is used to analyse the final shape of the irradiation product, which is then compared with the starting material. The optical absorption spectrum of the studied nanoparticles in colloidal or micellar solution can also be a very good indication of laser-induced structural changes as the plasmon resonance

depends on particle size and shape (see section 2). While lasers have been used in the production of nanoparticles [100, 185–190] the detailed study of the laser-induced nuclear changes of nanoparticles might allow one to shape the particles after production in a controlled manner independent of the synthetic method. In this way the discussion below might find many parallels in the broad field of laser ablation and processing of bulk materials or thin films [191–197].

In the case of spherical nanoparticles, Koda and co-workers [178, 179] reported that irradiation of gold particles in aqueous solution with 532 nm nanosecond laser pulses leads to fragmentation of the nanodots. This was explained in terms of the slow heat release of the deposited laser energy into the surrounding solvent, which leads to melting and even vaporization of the nanoparticles as estimated from the deposited laser energy and the absorption cross-section. Since the nanoparticles cannot cool as fast as they are heated, they fragment into smaller nanodots. The size reduction of silver nanoparticles in a glass matrix induced by excimer laser irradiation at 248 nm was also explained by a thermal model [180]. On the other hand, in a study of colloidal silver nanoparticles which were irradiated with 355 nm picosecond laser pulses, Kamat *et al.* [181] proposed that a transient aggregate is formed via photoejection of electrons after laser excitation, which is considered to be a precursor for complete fragmentation of the nanoparticles. Hence, the initial ejection of photoelectrons causes the particles to become positively charged and the repulsion between the charges then leads to fragmentation.

While high-energy laser pulses can induce a size reduction of nanodots, a more gentle melting of the spherical nanoparticles with lower pulse energies might remain unnoticed as the most thermodynamically favourable shape is the sphere itself. Even if the melting temperature of the material is reached and the nanoparticle becomes a liquid droplet, no shape transformation will occur in an isotropic medium. However, irradiation of gold nanorods with femtosecond laser pulses has given some interesting results [178]. It was found that the nanorods melt into nanodots in solution after excitation with femtosecond laser pulses having pulse energies in the microjoule range (less than 10 mJ cm^{-2}). This process is independent of the excitation wavelength, similar to the bleaching of the surface plasmon resonance as the absorbed photon energy is transferred into lattice vibrations on the picosecond time scale by electron–phonon relaxation processes independent of the electronic transitions involved initially (see discussion in section 4). Figures 13 (*a*) and (*b*) show the TEM images of a gold nanorod sample with a mean aspect ratio of 3.7 before and after irradiation respectively with 800 nm femtosecond laser pulses having a pulse energy of 40 J. While some nanodots are already present in the starting solution as impurities [44, 53], the final irradiation product consists of only spherical nanoparticles. The statistical size and shape analysis of the particles in these two solutions further reveals that the average volume of the nanodots in figure 13 (*b*) is comparable with the average volume of the nanorods in the original starting solution in figure 13 (*a*) [182]. This confirms that it is possible to melt the metal nanoparticles in aqueous solution by selectively exciting the electron gas of the metal nanoparticles with an intense femtosecond laser pulse and without fragmenting them by controlling the laser pulse energy.

The nanorod–nanodot shape transformation in solution is also reflected in the optical absorption data. While the transverse mode of the surface plasmon oscillation of gold nanorods coincides spectrally with the surface plasmon absorption of nanodots, the longitudinal mode is red-shifted and therefore characteristic for rod-

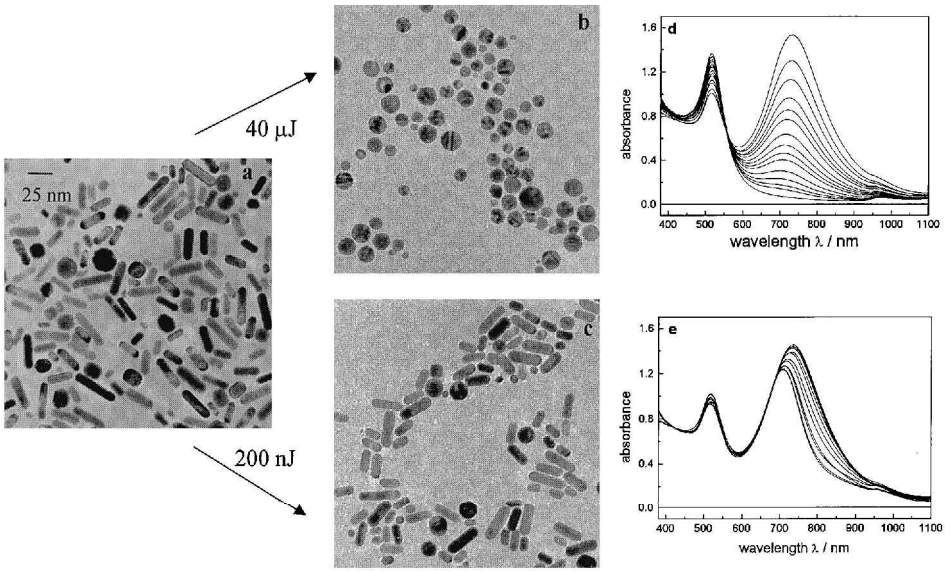

Figure 13. Photothermal reshaping of gold nanorods with femtosecond laser pulses. (*a*) TEM image of the original gold nanorods solution having a mean aspect ratio of 3·7. (*b*), (*c*) TEM images of the same nanorod solution after irradiation with 100 femtosecond laser pulses having a pulse energy of 40 and 200 nJ respectively. The wavelength of the laser light was at 800 nm, which falls within the broad absorption band of the longitudinal surface plasmon resonance. (*d*), (*e*) Each of the optical absorption spectra were recorded after an increased irradiation time and the TEM image to the left corresponds to the last absorption spectrum measured.

shaped nanoparticles [44, 47, 53]. Figure 13(*d*) shows the absorption spectra recorded after successive intervals of laser irradiation of a small amount of nanorod solution placed in a rotating cylindrical cell. The intensity of the longitudinal plasmon mode decreases evenly across the broad absorption band and all the nanorods in the starting solution are finally depleted. The intensity of the transverse mode increases at the same time, leading to the conclusion that the extinction coefficient of the transverse mode of nanorods is smaller than the extinction coefficient of the surface plasmon absorption of spherical nanoparticles [182]. Furthermore, the time dependences of these two spectral changes match, suggesting that the observed shape transformation for a single nanorod into a nanodot is completed by the interaction with only one laser pulse. The next laser pulse will simply be absorbed by other nanorods left in the solution but not by a previously excited nanorod as that has transformed into a spherical particle with no longitudinal surface plasmon absorption.

The situation is different when the laser pulse energy is lowered [182]. The lower half of figure 13 illustrates this case. The excitation energy is just 200 nJ. An optical hole can only be burned in the broad longitudinal plasmon band at the wavelength of the exciting laser pulse (figure 13(*e*)). The broad absorption band is due to the size distribution of the gold nanorods, which is considerably narrowed by removing the rods with the larger aspect ratios absorbing on the red edge of the absorption band [93]. Only the nanorods that absorb strongly at the excitation wavelength are heated sufficiently to undergo a shape transformation. The gentle surface melting of the nanorods leads to shorter but wider rods [11] as shown from the TEM image in figure

13(*c*) as well as the change in the mean nanorod aspect ratio, length and width upon laser irradiation as shown in figures 14(*a*), (*b*) and (*c*) respectively. The average aspect ratio of 3.7 has decreased to 2.7 after laser irradiation, which is due to a decrease in the average rod length from 31 to 25 nm and an increase in the average width from 8.4 to 9.4 nm. As the shorter nanorods are not intrinsically wider in the starting solution (as checked independently), these results are consistent with surface melting and inconsistent with depletion of the long nanorods due to complete melting into nanodots. The increase in the intensity at 520 nm suggests that spherical nanoparticles are also formed at the same time. In conclusion, this experiment narrows the initial size distribution of the starting gold nanorod sample considerably [182].

While the nanorod–nanodot shape transformation was followed by two steady-state techniques, namely TEM and ultraviolet–visible absorption spectroscopy, an interesting question arises as to how much time the actual shape transformation takes [198]. In order to answer this question, we used time-resolved pump–probe spectroscopy to monitor the rate of the disappearance of the longitudinal surface plasmon absorption after femtosecond pulsed photothermal heating of the nanorod solution [198]. The red wavelength absorption edge of the longitudinal plasmon absorption was chosen to monitor this process in order to avoid interference from the transient reversible bleach of this band upon excitation. At longer wavelengths, the bleach crosses over into an absorption in the transient spectrum and the bleach signal becomes very small [167], thus not interfering with a signal caused by the permanent bleaching of the longitudinal plasmon band due to the nanorod melting. The experiment was further carried out in a flow cell with a large sample volume in order to ensure that the overall percentage of nanorods destroyed remains small and that a new probe volume of a fresh (mainly unexposed) nanorod solution is sampled every laser pulse [198]. The result obtained from a gold nanorod sample with an average aspect ratio of 2.9 is shown in figure 15. The photothermal excitation wavelength was 400 nm with an energy of 9 μJ and the monitoring wavelength was 790 nm [198]. That nanodots are indeed produced was checked independently by TEM for a small amount of the nanorod solution which was placed in a rotating cylindrical cell and irradiated until the complete destruction of the longitudinal surface plasmon band was observed [198]. Figure 15 shows the rise in the permanent bleach signal, which is attributed to the disappearance of the plasmon band at this wavelength and hence marks the beginning of the shape transformation from a rod to a sphere. A fit of the data points gives a time of 30 ± 5 ps. This time gives the lower limit of the nanorod–nanodot transformation time since the monitoring wavelength was set to the red edge of the plasmon band. The measured transformation time is independent of the laser pump power in the investigated power range 5–20 μJ [198]. Only melting with no fragmentation occurs with the femtosecond laser pulses of these energies and a focus spot of about 100–200 μm. Furthermore, no significant dependence of the photoinduced isomerization dynamics on the gold nanorod aspect ratio could be detected for four samples with aspect ratios ranging from 1.9 to 3.7 [198].

It is worth noting that this transformation time is faster than the cooling of the gold lattice (greater than 100 ps [143–148, 164–167]) but slower than the electron–phonon relaxation time (less than 10 ps [143–148, 164–167]). This is expected from the discussion in section 4 about the energy relaxation in metal nanoparticles. In the case of laser irradiation with femtosecond laser pulses, the separation into sequential processes of excitation of the electron gas, lattice heating by electron–phonon coupling, and melting of the nanorods is justified. However, this is not valid any longer

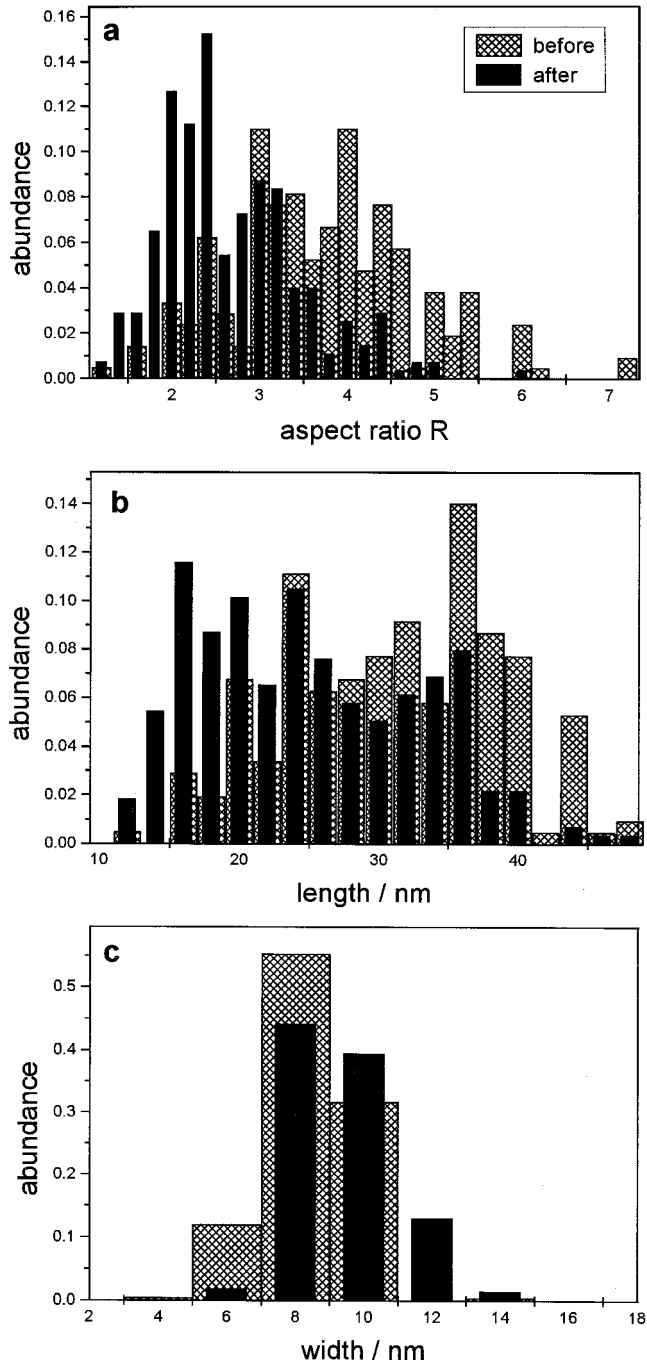

Figure 14. Laser-induced narrowing of the gold nanorod size distribution with low power femtosecond pulses. The statistical analysis of the nanorod solution irradiated with 200 nJ femtosecond laser pulses (see figures 13 (*c*) and 13 (*e*)) is shown. The distributions of (*a*) the aspect ratios, (*b*) the rod lengths and (*c*) the widths of the final product are compared with the original starting solution (see figure 13 (*a*)). The average aspect ratio decreases from 3·7 to 2·7 as the optical hole is created at the long-wavelength side corresponding to the rods with the largest aspect ratio. This is caused by a decrease in the nanorod length

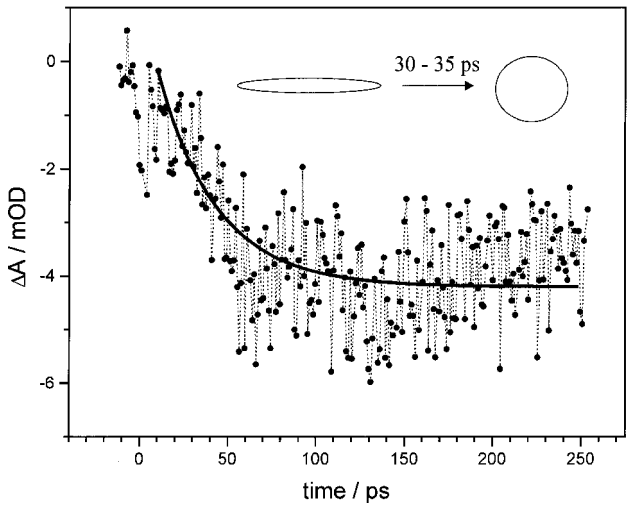

Figure 15. How long does it take to melt a gold nanorod? Transient absorption signal recorded at 790 nm where the longitudinal mode of the surface plasmon resonance absorption of gold nanorods having a mean aspect ratio of 2.9 nm is excited. The excitation wavelength was 400 nm and the pulse energy was 9 μJ, which is sufficient to melt the nanoparticles into spherical particles. The permanent bleach therefore corresponds to the shape transformation from rods to dots. The fit gives a transformation time of 30 ± 5 ps.

when a laser with a picosecond or nanosecond pulse duration is used. In fact, it is found that the final irradiation product can be quite different when a nanosecond laser is used as the irradiation source [182]. Comparing the influence of nanosecond with that of femtosecond laser pulses, it is found that the energy threshold for the complete melting of gold nanorods is lower with femtosecond laser pulses [199]. In figure 16 the optical absorption data and TEM images of a sample with a mean aspect ratio of 4.1 irradiated with laser pulses having the same laser pulse energy of 20 μJ (and fluence of 0.25 J cm^{-2}) but different laser pulse widths are shown (figures 16(*a*) and (*b*) show irradiation with femtosecond pulses, and figures 16(*c*) and (*d*) irradiation with nanosecond pulses). In the case of irradiation with nanosecond pulses, only an optical hole burning is observed similar to that observed when femtosecond pulses with much lower pulse energies (see figure 13(*e*)) are used. The dominant particle shape in the TEM image (figure 16(*d*)) is a ϕ-shaped nanoparticle (particle of mainly cylindrical shape with a spherical middle part), indicating that only partial melting occurs compared with the nanodots seen in figure 16(*b*) produced by irradiation with femtosecond laser pulses. Bent and twisted nanorods and especially ϕ-shaped particles are mainly found after irradiation with nanosecond pulses as independently reported by Chang *et al*. [183]. The same type of particles can also be observed with femtosecond irradiation but only at much lower pulse energies and with a lower abundance [199]. The ϕ-shaped particles seem to be an early stage of the shape transformation into spheres (i.e. melting) [183, 199] in which the pulse energy is not

---

from 31 to 25 nm while the width increases from 8.4 to 9.4 nm. As the shortest nanorods are not the widest rods in the starting solution, this result suggests that the nanorods undergo a surface melting in which the nanorods become wider at a cost to their length.

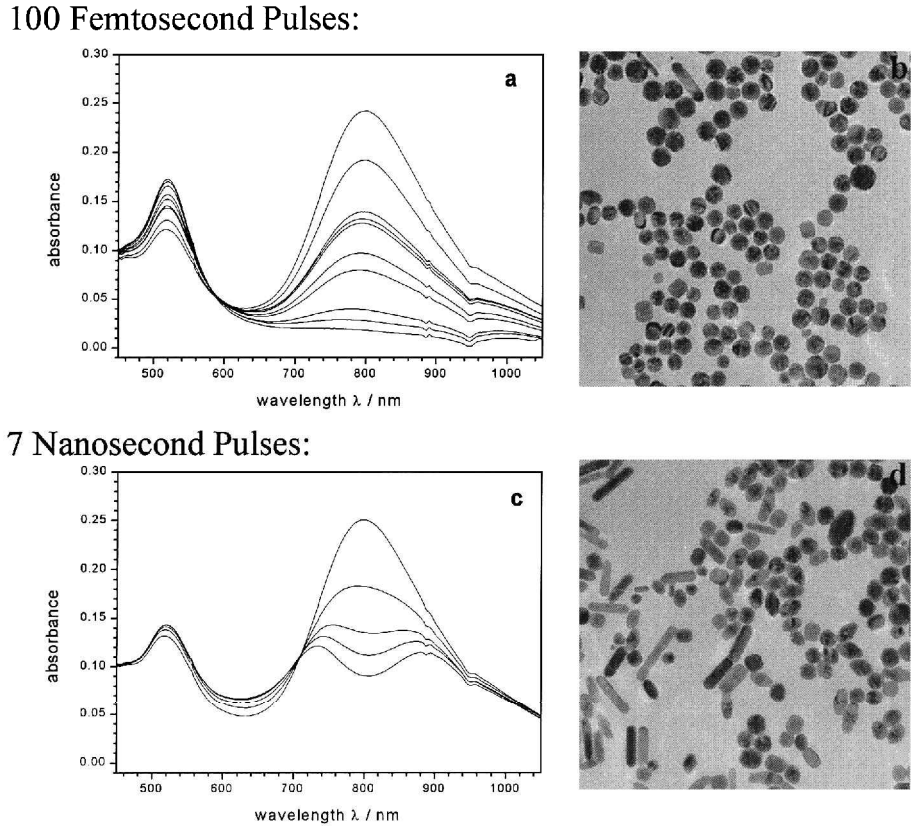

Figure 16. The effect of the laser pulse width on the photothermal reshaping of gold nanorods. The optical absorption data and TEM images of a nanorod sample with a mean aspect ratio of 4.1 irradiated by laser pulses having the same fluence (0.25 J cm^{-2}) but different laser pulse widths ((*a*), (*b*) 100 fs; (*c*), (*d*) 7 ns) are compared. A complete melting of the gold nanorods into spherical nanoparticles (concluded from the TEM picture) and a complete depletion of the nanorods (as seen in the final optical absorption spectrum) are achieved with femtosecond laser pulses. When nanosecond pulses of the same energy (fluence) are used, only an optical hole burning at the laser wavelength and a partial melting of the gold nanorods are found. A high abundance of ϕ-shaped particles is clearly visible. This result leads to the conclusion that nanosecond laser pulses are less effective in melting the gold nanorods.

high enough for complete melting as phonon–phonon coupling with the surrounding medium can partially compete with the nanoparticle heating by the laser energy. This further suggests that the nanorods cool most rapidly at their ends, where their exposed surface area is the largest [199]. This might also be the path of the photothermal isomerization process from rods to spheres in which the width of the rod increases around the middle of the rod, pulling the two ends closer to one another. (A high-resolution TEM study is now under way to examine the mechanism of melting [200].)

The difference in laser processing of gold nanorods with different laser pulse widths can be explained by the fact that the heat loss (phonon–phonon relaxation from the nanoparticle lattice to the solvent molecules) can effectively compete with the rate of heating the lattice. This is determined by the rate of photon absorption and the rate of electron–phonon relaxation. In the case of when a femtosecond laser pulse is used as

the excitation source, the photophysical events (absorption by the electrons, coupling to the lattice, melting and heat release to the solvent) are basically separated in time and could be thought of as sequential processes to a first approximation. This is certainly not justified for the nanosecond case. This is especially true in cases when the absorption coefficient of the gold nanorods at the excitation wavelength changes owing to shape changes. The longitudinal surface plasmon band bleaches because of the hot electron gas absorption, leading to a decrease in absorption and therefore to a less effective heating of the nanorods [167]. The difference in the energy threshold for observing a complete melting of the nanorods when the two lasers are used can now be understood [199]. Melting occurs if the rate of heating the lattice is faster than the rate of cooling the lattice. With femtosecond lasers the laser intensity is so high that the rate of absorption (and thus heating) is very rapid. Therefore, the same number of photons squeezed in 100 fs can heat the lattice much more effectively and more rapidly than if they are stretched to a nanosecond pulse width.

When nanosecond laser pulses of higher energies (millijoule range) are used, fragmentation of the gold nanorods into smaller, nearly spherical nanoparticles is observed [182] similar to those observed for the gold [178, 179] and silver [180, 181] nanodots described above. While this observation was explained for the nanodots in terms of the slow heat loss to the solvent or the ejection of photoelectrons, for a gold nanorod solution another mechanism was shown to contribute as well [182]. As the nanorods' lattice heats up and melts during the long nanosecond laser pulse, the gold nanoparticle continues to absorb photons. The additional photons absorbed by the hot particles was proposed to lead to fragmentation of the gold nanorods [182]. This model can be described as follows:

$$(\mathrm{Au})_{\mathrm{NR}} \xrightarrow{nh\nu} [(\mathrm{Au})_{\mathrm{NR}}]^{\#}, \tag{5.1}$$

$$[(\mathrm{Au})_{\mathrm{NR}}]^{\#} \xrightarrow{\mathrm{fs}} [(\mathrm{Au})_{\mathrm{NR}}]^{\perp}, \tag{5.2}$$

$$[(\mathrm{Au})_{\mathrm{NR}}]^{\perp} \xrightarrow{\mathrm{ps}} [(\mathrm{Au})_{\mathrm{NR}}]^{\mathrm{vib}*}, \tag{5.3}$$

$$[(\mathrm{Au})_{\mathrm{NR}}]^{\mathrm{vib}*} \xrightarrow{\mathrm{melting}} [(\mathrm{Au})_{\mathrm{NS}}], \tag{5.4}$$

$$[(\mathrm{Au})_{\mathrm{NP}}]^{\mathrm{vib}*} \xrightarrow{mh\nu\,(\mathrm{ns})} [(\mathrm{Au})_{\mathrm{NP}}]^{\mathrm{vib}**}, \tag{5.5}$$

$$[(\mathrm{Au})_{\mathrm{NP}}]^{\mathrm{vib}**} \xrightarrow{\mathrm{fragmentation}} (\mathrm{Au})_{\mathrm{SNS}}. \tag{5.6}$$

Processes (5.1), (5.2) and (5.3) represent laser excitation of the electrons, thermal heating of the electrons (less than 1 ps [166]), and lattice heating resulting from electron–phonon relaxation processes (less than 10 ps [143–149, 164–167]) respectively. NR, NS, NP and SNS refer to nanorods, nanospheres, nanoparticles (when there is no definite information about the particle shape) and small nanospheres respectively. It is important to note that heating the lattice via electron–phonon relaxation in the femtosecond experiment occurs in the dark, as it takes place on a time scale longer than the pulse width. Process (5.4) is the melting of the nanorods, which completes the photophysical events in the femtosecond experiment if heat loss to the surrounding medium is neglected. However, this is not the case for the nanosecond experiments. Process (5.5) represents further laser excitation of the hot lattice in the experiments with nanosecond laser pulses. Therefore it is expected that absorption of

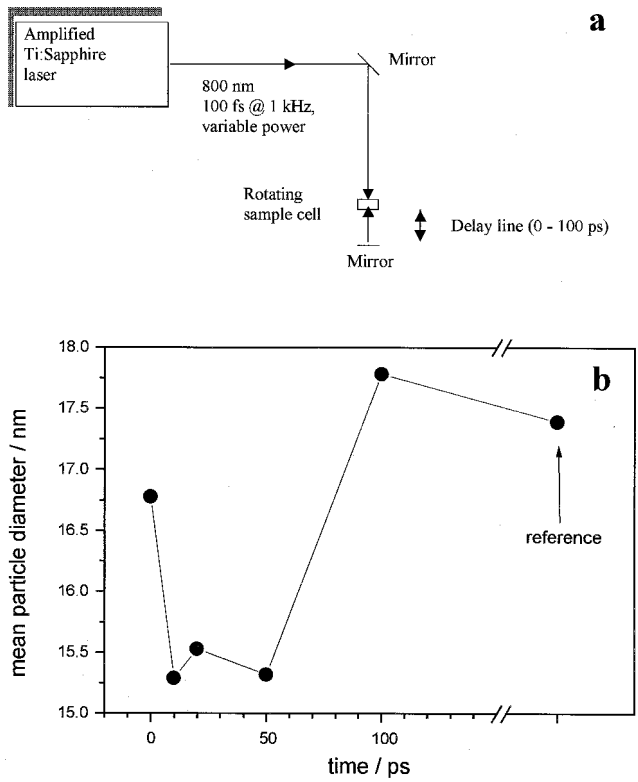

Figure 17. Gold nanorod fragmentation caused by two time-delayed femtosecond pulses serving as a model for a longer (nanosecond) laser pulse. (*a*) The set-up used for performing the irradiation of gold nanoparticle solutions with two time-delayed laser pulses. The gold nanorod solution placed in a rotating cylindrical cell is first irradiated by a laser pulse and then the transmitted light is retroreflected into the solution and overlapped with the first excitation spot. The second pulse can be delayed with respect to the first by a variable translation stage. In this way a longer laser pulse is simulated by two ultrashort laser pulses in order to test the influence of the pulse duration on the shape transformation of gold nanorods. The delay time used is bracketing the electron–phonon and phonon–phonon relaxation time of gold nanorods in solution. (*b*) The average particle diameter of the spheres produced by the laser irradiation plotted against the delay time between the two pulses. At delay times between 10 and 50 ps a smaller average particle diameter is observed owing to a higher abundance of smaller nanoparticles, which are created by fragmentation of the gold nanorods. With knowledge of the lattice heating and cooling dynamics this confirms the proposed mechanism that fragmentation of the gold nanorods with nanosecond laser pulses occurs because of the additional absorption of photons by the hot (melted) lattice during the duration of the nanosecond pulse.

more photons by the hot (or even melted) lattice occurs in the nanosecond experiment. This then leads to an increase in the lattice internal energy and finally fragmentation as shown in step (5.6).

In order to test this mechanism, the gold nanorods were irradiated in solution by two femtosecond pulses which were delayed by different amounts of time with respect to each other [182]. The first pulse initially excites the nanorods and heats their lattice while the second pulse is absorbed at different stages of excitation and relaxation after the absorption of the first pulse. The mean diameter of the resulting particles is

determined by using TEM of the dried solutions of the nanoparticles taken from the solution exposed to the two pulses separated by different delay times. A schematic diagram of the set-up for this experiment is shown in figure 17(*a*) and the results are given in figure 17(*b*). The average particle diameter of the nanoparticles produced by the laser irradiation is plotted against the delay time between the two pulses. The point labelled as reference refers to a control experiment in which the mirror behind the sample cell was removed and therefore just one pulse was passed through the sample. Only melting of the nanorods into spherical nanoparticles is observed. It was further observed that a single pulse having the same energy as the sum of the two individual laser pulses did not lead to a different mean particle diameter. At delay times between 10 and 50 ps, a smaller average particle diameter is observed owing to a higher abundance of smaller nanoparticles which originate from the fragmentation of the gold nanorods. At shorter delay times than the electron–phonon relaxation time (a few picoseconds), the lattice of the nanorods has not yet been completely heated or melted before the second pulse arrives. At delay times longer than phonon–phonon relaxation times (greater than 100 ps), the lattice has already cooled considerably by phonon–phonon interactions. Fragmentation is hence only observed when the second laser pulse is absorbed after the lattice is heated (and melted) and before it cools. This supports the suggested mechanism of the fragmentation of gold nanorods induced by lasers of energetic long (nanosecond) laser pulses.

6. Concluding remarks and outlook

This review of the optical and dynamic properties of gold nanocrystals shows that a great deal of understanding has already been accomplished. The understanding of the dynamics of the electrons and the lattice of nanostructured materials is of great importance to their potential use in future photonic applications. The sensitivity of the surface plasmon absorption characteristics to adsorbed species is important for their potential applications as chemical sensors. The understanding of the laser-induced photothermal melting and fragmentation mechanisms will be helpful in future photothermal reshaping of metal nanoparticles.

The understanding of the electronic absorption and dynamics in individual nanoparticles is essential before we assemble them into devices, which is the goal of the use of nanostructured systems. The advancements in chemical synthesis and separation methods are pushing the limits of preparing and isolating nanoparticles of different size and shape. The study of a sample with a narrow size and shape distribution is essential in determining the physical and especially the optical properties of individual particles in an assembled mixture. Single-particle spectroscopy could overcome the problem of a narrow size distribution but is mainly limited to collecting the emission rather than measuring the absorption spectrum. On the other hand, a great effort has been made to try to create assemblies of nanoparticles in two- and three-dimensional structures [70–72, 201–209]. Deoxyribonucleic acid [201] or smaller molecules [202] and also templates such as aluminium oxide membranes [203] have been used to create linked arrays of gold nanoparticles. Lithography [70–72, 204] and electrophoretic deposition [205] also allow the two-dimensional arrangement of metallic particles. The patterning of structures consisting of individual and well separated nanoparticles as solid-state devices is crucial for any future application. In order to self-assemble nanoparticles, the size distribution needs to be very narrow so that the goals of both preparing a monodisperse sample and assembling the nanoparticles are very closely related. This in turn presents the prospect of observing new optical properties of self-

assembled monolayers of metallic nanoparticles as now the electric fields connected to the plasmon resonance (enhancement of the incoming and outgoing electric fields when interacting with light) will influence the effective fields around the neighbouring nanoparticles. Although aggregates of metallic nanoparticles [94–96] and their optical absorption have been studied experimentally and theoretically, an ordered array of nanoparticles instead of an agglomerate might present new properties different from the individual particles.

Acknowledgements

We wish to acknowledge our collaborators Professor Zhong L. Wang, Dr Clemens Burda, Mona M. Mohamed, Babak Nikoobakht and Victor Volkov. We would like to thank Janet Petroski for carefully reading the manuscript. This work was supported by the National Science Foundation (grant CHE 9705164).

References

[1] Henglein, A., 1993, *J. phys. Chem.*, **97**, 8457.
[2] Henglein, A., 1989, *Chem. Rev.*, **89**, 1861.
[3] Alivisatos, A. P., 1996, *J. phys. Chem.*, **100**, 13 226.
[4] Mulvaney, P., 1996, *Langmuir*, **12**, 788.
[5] Storhoff, J. J., and Mirkin, C. A., 1999, *Chem. Rev.*, **99**, 1849.
[6] Schmid, G., and Chi, L. F., 1998, *Adv. Mater.*, **10**, 515.
[7] Alivisatos, A. P., Barbara, P. F., Castleman, A. W., Chang, J., Dixon, D. A., Klein, M. L., McLendon, G. L., Miller, J. S., Ratner, M. A., Rossky, P. J., Stupp, S. I., and Thompson, M. E., 1998, *Adv. Mater.*, **10**, 1297.
[8] Wang, Y., and Herron, N., 1991, *J. phys. Chem.*, **95**, 525.
[9] Heath, J. R., and Shiang, J. J., 1998, *Chem. Soc. Rev.*, **27**, 65.
[10] Weller, H., 1993, *Angew. Chem., Int. Edn Engl.*, **32**, 41.
[11] Link, S., and El-Sayed, M. A., 1999, *J. phys. Chem.* B, **103**, 8410.
[12] Schmid, G., 1994, *Clusters and Colloids: From Theory to Application* (Weinheim: VCH).
[13] Kamat, P. V., and Meisel, D., 1997, *Studies in Surface Science and Catalysis*, Vol. 103, *Semiconductor Nanoclusters—Physical, Chemical, and Catalytic Aspects* (Amsterdam: Elsevier).
[14] Edelstein, A. S., and Cammarata, R. C., 1996, *Nanoparticles: Synthesis, Properties and Applications* (Bristol: Institute of Physics).
[15] Kerker, M., 1985, *J. Colloid Interface Sci.*, **105**, 297.
[16] Creighton, J. A., and Eadon, D. G., 1991, *J. chem. Soc., Faraday Trans.*, **87**, 3881.
[17] Hughes, A. E., and Jain, S. C., 1979, *Adv. Phys.*, **28**, 717.
[18] Faraday, M., 1857, *Phil. Trans. R. Soc.*, **147**, 145.
[19] Mie, G., 1908, *Ann. Phys.*, **25**, 329.
[20] Graetzel, M., 1992, *Electrochemistry in Colloids and Dispersions*, edited by R. A. Mackay and J. Texter (Weinheim: VCH).
[21] Perenboom, J. A. A. J., Wyder, P., and Meier, P., 1981, *Phys. Rep.*, **78**, 173.
[22] Halperin, W. P., 1986, *Rev. mod. Phys.*, **58**, 533.
[23] Kreibig, U., and Vollmer, M., 1995, *Optical Properties of Metal Clusters* (Berlin: Springer).
[24] Brus, L. E., 1983, *J. chem. Phys.*, **79**, 5566.
[25] Brus, L. E., 1984, *J. chem. Phys.*, **80**, 4403.
[26] Brus, L. E., 1991, *Appl. Phys.* A, **53**, 465.
[27] Murray, C. B., Norris, D. J., and Bawendi, M. G., 1993, *J. Am. chem. Soc.*, **11**, 8706.
[28] Whetten, R. L., Khoury, J. T., Alvarez, A. M., Murthy, S., Vezmar, I., Wang, Z. L., Stephens, P. W., Cleveland, C. L., Luedtke, W. D., and Landman, U., 1996, *Adv. Mater.*, **8**, 428.
[29] Chemseddine, A., and Weller, H., 1993, *Ber. Bunsenges. phys. Chem.*, **97**, 636.
[30] Ahmadi, T. S., Wang, Z. L., Green, T. C., and El-Sayed, M. A., 1996, *Science*, **272**, 1924.
[31] Brust, M., Walker, M., Bethell, D., Schiffrin, D. J., and Wyhnman, R., 1994, *J. chem. Soc., chem. Commun.*, 801.

[32] HOSTETLER, M. J., WINGATE, J. E., ZHONG, C.-J., HARRIS, J. E., VACHET, R. W., CLARK, M. R., LONDONO, J. D., GREEN, S. J., STOKES, J. J., WIGNALL, G. D., GLISH, G. L., PORTER, M. D., EVANS, N. D., and MURRAY, R. W., 1998, *Langmuir*, **14**, 17.
[33] HANDLEY, D. A., 1989, *Colloidal Gold: Principles, Methods, and Applications*, Vol. 1 (New York: Academic Press).
[34] TURKEVICH, J., STEVENSON, P. C., 19 Hillier, J., 1951, *Discuss. Faraday Soc.*, **11**, 55.
[35] TURKEVICH, J., GARTON, G., and STEVENSON, P. C., 1954, *J. Colloid Sci., Suppl.*, **1**, 26.
[36] TURKEVICH, J., 1985, *Gold Bull.*, **18**, 86.
[37] TURKEVICH, J., 1985, *Gold Bull.*, **18**, 125.
[38] TANO, T., ESUMI, K., and MEGURO, K., 1989, *J. Colloid Interface Sci.*, **133**, 530.
[39] ESUMI, K., SUZUKI, M., TANO, T., TORIGOE, K., and MEGURO, K., 1991, *Colloids Surf.*, **55**, 9.
[40] ESUMI, K., SADAKANE, O., TORIGOE, K., and MEGURO, K., 1992, *Colloids Surf.*, **62**, 255.
[41] ESUMI, K., TANO, T., and MEGURO, K., 1989, *Langmuir*, **5**, 268.
[42] TOSHIMA, N., TAKAHASHI, T., and HIRAI, H., 1985, *Chem. Lett.*, 1245.
[43] REETZ, M. T., and HELBIG, W., 1994, *J. Am. chem. Soc.*, **116**, 7401.
[44] YU, Y., CHANG, S., LEE, C., and WANG, C. R. C., 1997, *J. phys. Chem.* B, **101**, 34, 6661.
[45] BLACKBOROW, J. R., and YOUND, D., 1979, *Metal Vapor Synthesis* (New York: Springer).
[46] DOREMUS, R. H., 1964, *J. chem. Phys.*, **40**, 2389.
[47] VAN DER ZANDE, B. M. I., BOHMER, M. R., FOKKINK, L. G. J., and SCHONENBERGER, C., 1997, *J. phys. Chem.* B, **101**, 852.
[48] FOSS, C. A., HORNYAK, G. L., TIERNEY, M. J., and MARTIN, C. R., 1992, *J. phys. Chem.*, **96**, 9001.
[49] HORNYAK, G. L., PATRISSI, C. J., and MARTIN, C. R., 1997, *J. phys. Chem.* B, **101**, 1548.
[50] FOSS, C. A., HORNYAK, G. L., STOCKERT, J. A., and MARTIN, C. R., 1992, *J. phys. Chem.*, **96**, 7497.
[51] FOSS, C. A., HORNYAK, G. L., STOCKERT, J. A., and MARTIN, C. R., 1994, *J. phys. Chem.*, **98**, 2963.
[52] HORNYAK, G. L., and MARTIN, C. R., 1997, *Thin Solid Films*, **303**, 84.
[53] MOHAMED, M. B., ISMAEL, K. Z., LINK, S., and EL-SAYED, M. A., 1998, *J. phys. Chem.* B, **102**, 9370.
[54] LISIECKI, I., BILLOUDET, F., and PILENI, M. P., 1996, *J. phys. Chem.*, **100**, 4160.
[55] LISIECKI, I., and PILENI, M. P., 1993, *J. am. Chem. Soc.*, **115**, 3887.
[56] LINK, S., and EL-SAYED, M. A., 1999, *J. phys. Chem.* B, **103**, 4212.
[57] MAXWELL-GARNETT, J. C., 1904, *Phil. Trans. R. Soc.*, **203**, 385.
[58] PAPAVASSILIOU, G. C., 1980, *Prog. solid st. Chem.*, **12**, 185.
[59] KERKER, M., 1969, *The Scattering of Light and Other Electromagnetic Radiation* (New York: Academic Press).
[60] BOHREN, C. F., and HUFFMAN, D. R., 1983, *Absorption and Scattering of Light by Small Particles* (New York: Wiley).
[61] NOZIK, A. J., and MEMMING, R., 1996, *J. phys. Chem.*, **100**, 13061.
[62] SCHAAFF, T. G., KNIGHT, G., SHAFIGULLIN, M., BORKMAN, R. F., and WHETTEN, R. L., 1998, *J. phys. Chem.* B, **102**, 10643.
[63] KREIBIG, U., and GENZEL, U., 1985, *Surf. Sci.*, **156**, 678.
[64] ALVAREZ, M. M., KHOURY, J. T., SCHAAFF, T. G., SHAFIGULLIN, M. N., VEZMER, I., and WHETTEN, R. L., 1997, *J. phys. Chem.* B, **101**, 3706.
[65] SCHAAFF, T. G., SHAFIGULLIN, M. N., KHOURY, J. T., VEZMER, I., WHETTEN, R. L., CULLEN, W. G., FIRST, P. N., GUTIERREZ-WING, C., ASCENSIO, J., and JOSE-YACAMAN, M. J., 1997, *J. phys. Chem.* B, **101**, 7885.
[66] HEILWEIL, E. J, and HOCHSTRASSER, R. M., 1985, *J. chem. Phys.*, **82**, 4762.
[67] KREIBIG, U., GARTZ, M., and HILGER, A., 1997, *Ber. Bunsenges. phys. Chem.*, **101**, 1593.
[68] PUECH, K., HENARI, F. Z., BLAU, W. J., DUFF, D., and SCHMID, G., 1995, *Chem. Phys. Lett.*, **247**, 13.
[69] PUECH, K., HENARI, F. Z., BLAU, W. J., DUFF, D., and SCHMID, G., 1995, *Europhys. Lett.*, **32**, 119.
[70] LAMPRECHT, B., LEITNER, A., and AUSSENEGG, F. R., 1997, *Appl. Phys.* B, **64**, 269.
[71] LAMPRECHT, B., KRENN, J. R., LEITNER, A., and AUSSENEGG, F. R., 1999, *Appl. Phys.* B, **69**, 223.

[72] Lamprecht, B., Leitner, A., and Aussenegg, F. R., 1999, *Appl. Phys.* B, **68**, 419.
[73] Klar, T., Perner, M., Grosse, S., von Plessen, G., Spirkl, W., and Feldmann, J., 1998, *Phys. Rev. Lett.*, **80**, 4249.
[74] Kreibig, U., and von Fragstein, C., 1969, *Z. Phys.*, **224**, 307.
[75] Kreibig, U., 1970, *Z. Phys.*, **234**, 307.
[76] Ashcroft, N. W., and Mermin, N. D., 1976, *Solid State Physics* (Philadelphia, Pennsylvania: Saunders College).
[77] Doremus, R. H., 1965, *J. chem. Phys.*, **42**, 414.
[78] Smithard, M. A., 1974, *Solid St. Commun.*, **14**, 407.
[79] Ruppin, R., and Yatom, H., 1976, *Phys. Stat. sol.* (b), **74**, 647.
[80] Kawabata, A., and Kubo, R., 1966, *J. phys. Soc. Japan*, **21**, 1765.
[81] Hache, F., Ricard, D., and Flytzanis, C., 1986, *J. opt. Am. Soc.* B, **3**, 1647.
[82] Cini, M., 1987, *J. opt. Soc. Am.*, **71**, 386.
[83] Genzel, L., Martin, T. P., and Kreibig, U., 1975, *Z. Phys.* B, **21**, 339.
[84] Wood, D. M., and Ashcroft, N. W., 1982, *Phys. Rev.* B, **25**, 6255.
[85] Kraus, W. A., and Schatz, G. C., 1983, *J. chem. Phys.*, **79**, 6130.
[86] Yannouleas, C., and Broglia, R. A., 1992, *Ann. Phys.*, **217**, 105.
[87] Brack, M., 1993, *Rev. mod. Phys.*, **65**, 677.
[88] Bonacic-Koutecky, V., Fantucci, P., and Koutecky, J., 1991, *Chem. Rev.*, **91**, 1035.
[89] Persson, N. J., 1993, *Surf. Sci.*, **281**, 153.
[90] Linnert, T., Mulvaney, P., and Henglein, A., 1993, *J. phys. Chem.*, **97**, 679.
[91] Hoevel, H., Fritz, S., Hilger, A., Kreibig, U., and Vollmer, M., 1993, *Phys. Rev.* B, **48**, 18178.
[92] Lyon, L. A., Musick, M. D., Smith, P. C., Reiss, B. D., Pena, D. J., and Natan, M. J., 1999, *Sensors Actuators* B, **54**, 118.
[93] Link, S., Mohamed, M. B., and El-Sayed, M. A., 1999, *J. phys. Chem.* B, **103**, 3073.
[94] Gans, R., 1915, *Annln Phys.*, **47**, 270.
[95] Kreibig, U., Althoff, A., and Pressmann, H., 1981, *Surf. Sci.*, **106**, 308.
[96] Quinten, M., and Kreibig, U., 1986, *Surf. Sci.*, **172**, 557.
[97] Quinten, M., Schoenauer, D., Kreibig, U., 1989, *Z. Phys.* D, **26**, 239.
[98] Aspnes, D. E., Heller, A., and Porter, J. D., 1986, *J. appl Phys.*, **60**, 3028.
[99] Aspnes, D. E., 1982, *Thin Solid Films*, **89**, 249.
[100] Palpant, B., Prevel, B., Lerme, J., Cottancin, E., Pellarin, M., Treilleux, M., Perez, A., Vialle, J. L., and Broyer, M., 1998, *Phys. Rev.* B, **57**, 1963.
[101] Mooradian, A., 1969, *Phys. Rev. Lett.*, **22**, 185.
[102] Whittle, D. G., and Burstein, E., 1981, *Bull. Am. phys. Soc.*, **26**, 777.
[103] Boyd, G. T., Yu, Z. H., and Shen, Y. R., 1986, *Phys. Rev.* B, **33**, 7923.
[104] Moshovists, M., 1985, *Rev. mod. Phys.*, **57**, 783.
[105] Heritage, J. P., Bergman, J. G., Pinczuk, A., and Worlock, J. M., 1979, *Chem. Phys. Lett.*, **67**, 229.
[106] Apell, P., and Monreal, R., 1988, *Physica Scripta*, **38**, 174.
[107] Plekhanov, V. G., and Siliukova, T. V., 1990, *Soviet Phys. Solid St.*, **32**, 1268.
[108] Chen, C. K., Heinz, T. F., Ricard, D., and Shen, Y. R., 1983, *Phys. Rev.* B, **27**, 1965.
[109] Boyd, G. T., Rasing, T., Leite, J. R. R., and Shen, Y. R., 1984, *Phys. Rev.* B, **30**, 519.
[110] Otto, A., 1991, *J. Raman Spectrosc.*, **22**, 743.
[111] Otto, A., Mrozek, I., Grabhorn, H., and Akeman, W., 1992, *J. Phys.: condens. Matter,* **4**, 1143.
[112] Zeman, E. J., and Schatz, G. C., 1987, *J. phys. Chem.*, **91**, 634.
[113] Cline, M. P., Barber, P. W., and Chang, R. K., 1986, *J. opt. Soc. Am.* B, **3**, 15.
[114] Creighton, J. A., Blatchford, C. G., and Albrecht, M. G., 1979, *J. chem. Soc., Faraday Trans. II*, **75**, 790.
[115] Kerker, M., Siiman, O., Bumm, L. A., and Wang, W.-S., 1980, *Appl. Optics*, **19**, 3253.
[116] Kerker, M., Wang, D., and Chew, H., 1980, *Appl. Optics*, **19**, 4159.
[117] Freeman, R. G., Hommer, M. B., Grabar, K. C., Jackson, M. A., and Natan, M. J., 1996, *J. phys. Chem.*, **100**, 718.
[118] Emory, S. R., Haskins, W. E., Nie, S., 1998, *J. Am. chem. Soc.*, **120**, 8009.
[119] Mohamed, M. B., Volkov, V. V., Links, S., and El-Sayed, M. A., 2000, *Chem. Phys. Lett.*, **317**, 517.

[120] Wilcoxon, J. P., Martin, J. E., Parsapour, F., Wiedenman, B., and Kelley, D. F., 1998, *J. chem. Phys.*, **108**, 9137.
[121] Esley, G. L., 1983, *Phys. Rev. Lett.*, **51**, 2140.
[122] Esley, G. L., 1986, *Phys. Rev.* B, **33**, 2144.
[123] Groeneveld, R. H. M., Sprik, R., and Lagendijk, A., 1992, *Phys. Rev.* B, **45**, 5079.
[124] Groeneveld, R. H. M., Sprik, R., and Lagendijk, A., 1995, *Phys. Rev.* B, **51**, 11 433.
[125] Schoenlein, R. W., Lin, W. Z., Fujimoto, J. G., and Esley, G. L., 1987, *Phys. Rev. Lett.*, **58**, 1680.
[126] Brorson, S. D., Fujimoto, J. G., and Ippen, E. P., 1987, *Phys. Rev. Lett.*, **59**, 1962.
[127] Sun, C.-K., Vallee, F., Acioli, L. H., Ippen, E. P., and Fujimoto, J. G., 1993, *Phys. Rev.* B, **48**, 12 365.
[128] Sun, C.-K., Vallee, F., Acioli, L. H., Ippen, E. P., and Fujimoto, J. G., 1994, *Phys. Rev.* B, **50**, 15 337.
[129] del Fatti, N., Bouffanais, R., Vallee, F., and Flytzanis, C., 1998, *Phys. Rev. Lett.*, **81**, 922.
[130] Elsayed-Ali, H. E., Juhasz, T., Smith, G. O., and Bron, W. E., 1991, *Phys. Rev.*B, **43**, 4488.
[131] Juhasz, T., Elsayed-Ali, H. E., Hu, H., and Bron, W. E., 1992, *Phys. Rev.* B, **45**, 13 819.
[132] Juhasz, T., Elsayed-Ali, H. E., Smith, G. O., Suarez, C., and Bron, W. E., 1993, *Phys. Rev.* B, **48**, 15 488.
[133] Fann, W. S., Storz, R., Tom, H. W. K., and Boker, J., 1992, *Phys. Rev.* B, **46**, 13 592.
[134] Fann, W. S., Storz, R., Tom, H. W. K., and Boker, J., 1992, *Phys. Rev. Lett.*, **68**, 2834.
[135] Schmuttenmaer, C. A., Aeschlimann, M., Elsayed-Ali, H. E., Miller, R. J. D., Mantell, D. A., Cao, J., and Gao, Y., 1994, *Phys. Rev.* B, **50**, 8957.
[136] Aeschlimann, M., Schmuttenmaer, C. A., Elsayed-Ali, H. E., Miller, R. J. D., Cao, J., Gao, Y., and Mantell, D. A., 1995, *J. chem. Phys.*, **102**, 8606.
[137] Gao, Y., Cao, J., Miller, R. J. D., Elsayed-Ali, H. E., and Mantell, D. A., 1997, *Phys. Rev.* B, **56**, 1099.
[138] Cao, J., Gao, Y., Elsayed-Ali, H. E., Miller, R. J. D., and Mantell, D. A., 1998, *Phys. Rev.* B, **58**, 10 948.
[139] Anisimov, L., Kapeliovich, B. L., and Perel'man, T. L., 1975, *Soviet Phys. JETP*, **39**, 375.
[140] Pawlik, S., Bauer, M., and Aeschlimann, M., 1997, *Surf. Sci.*, **377–379**, 206.
[141] Aeschlimann, M., Pawlik, S., and Bauer, M., 1995, *Ber. Bunsenges. phys. Chem.*, **99**, 1504.
[142] Ogawa, S. and Petek, H., 1996, *Surf. Sci.*, **357–358**, 585.
[143] Perner, M., Bost, P, Pauck, T., von Plessen, G., Feldmann, J., Becker, U., Mennig, M., Porstendorfer, J., Schmitt, M., and Schmidt, H., 1996, *Ultrafast Phenomena* X, edited by P. F. Babara, J. G. Fujimoto, W. H. Knox and W. Zinth (Berlin: Springer).
[144] Perner, M., Bost, P., von Plessen, G., Feldmann, J., Becker, U., Mennig, M., and Schmidt, H., 1997, *Phys. Rev. Lett.*, **78**, 2192.
[145] Perner, M., Klar, T., Grosse, S., Lemmer, U., von Plessen, G, Spirkl, W., and Feldmann, J., 1998, *J. Lumin.*, **76–77**, 181.
[146] Hodak, J. K., Martini, I., and Hartland, G. V., 1998, *Chem. Phys. Lett.*, **284**, 135.
[147] Hodak, J. K., Martini, I., and Hartland, G. V., 1998, *J. phys. Chem.* B, **102**, 6958.
[148] Hodak, J. K., Martini, I., and Hartland, G. V., 1998, *J. chem. Phys.*, **108**, 9210.
[149] Hodak, J. K., Henglein, A., and Hartland, G. V., 1999, *J. chem. Phys.*, **111**, 8613.
[150] Bigot, J.-Y., Merle, J.-C., Cregut, O., and Daunois, A., 1995, *Phys. Rev. Lett.*, **75**, 4702.
[151] Shahbazyan, T. V., Perakis, I. E., and Bigot, J.-Y., 1998, *Phys. Rev. Lett.*, **81**, 3120.
[152] Roberti, T. W., Smith, B. A., and Zhang, J. Z., 1995, *J. chem. Phys.*, **102**, 3860.
[153] Smith, B. A., Waters, D. M., Faulhaber, A. E., Kreger, M. A., Roberti, T. W., and Zhang, J. Z., 1997, *J. Sol–Gel Sci. Technol.*, **9**, 125.
[154] Faulhaber, A. E., Smith, B. A., Andersen, J. K., and Zhang, J. Z., 1996, *Molec. Crystals liq. Crystals*, **283**, 25.
[155] Smith, B. A., Zhang, J. Z., Giebel, U., and Schmid, G., 1997, *Chem. Phys. Lett.*, **270**, 139.
[156] Hamanaka, Y., Hayashi, N., Nakamura, A., and Omi, S., 1998, *J. Lumin.*, **76–77**, 221.

[157] Del Fatti, N., Tzortzakis, S., Voisin, C., Flytzanis, C., and Vallee, F., 1999, *Physica* B, **263–264**, 54.
[158] Del Fatti, N., Voisin, C., Chevy, F., Vallee, F., and Flytzanis, C., 1999, *J. chem. Phys.*, **110**, 484.
[159] del Fatti, N., Flytzanis, C., and Vallee, F., 1999, *Appl. Phys.* B, **68**, 433.
[160] Feldstein, M. J., Keating, C. D., Liau, Y.-H., Natan, M. J., and Scherer, N. F., 1997, *J. Am. chem. Soc.*, **119**, 6638.
[161] Inouye, H., Tanaka, K., Tanahashi, I., and Hirao, K., 1998, *Phys. Rev.* B, **57**, 11 334.
[162] Tokizaki, T., Nakamura, A., Kaneko, S., Uchida, K., Omi, S., Tanji, H., and Asahara, Y., 1994, *Appl. Phys. Lett.*, **65**, 941.
[163] Averitt, R. D., Westcott, S. L., and Halas, N. J., 1998, *Phys. Rev.* B, **58**, 10 203.
[164] Ahmadi, T. S., Logunov, S. L., and El-Sayed, M. A., 1996, *J. phys. Chem.*, **100**, 8053.
[165] Ahmadi, T. S., Logunov, S. L., El-Sayed, M. A., Khoury, J. T., and Whetten, R. L., 1997, *J. phys. Chem.* B, **101**, 3713.
[166] Link, S., Burda, C., Wang, Z. L., and El-Sayed, M. A., 1999, *J. chem. Phys.*, **111**, 1255.
[167] Link, S., Burda, C., Mohamed, M. B., Nikoobakht, B., and El-Sayed, M. A., 2000, *Phys. Rev.* B, **61**, 6086.
[168] Rosei, R., Antongeli, F., and Grassano, U. M., 1973, *Surf. Sci.*, **37**, 689.
[169] Cardona, M., 1969, *Modulation Spectroscopy*, Solid State Physics, Supplement II, edited by F. Seitz, D. Turnball and H. Ehrenreich (New York: Academic Press).
[170] Pines, D., and Nozières, P., 1966, *The Theory of Quantum Liquids* (New York: Benjamine).
[171] Christensen, N. E., and Seraphin, B. O., 1971, *Phys. Rev.* B, **4**, 3321.
[172] Stella, A., Nisoli, M., de Silvestri, S., Svelto, O., Lanzani, G., Cheyssac, P., and Kofman, R., 1996, *Phys. Rev.* B, **53**, 15 497.
[173] Stella, A., Nisoli, M., de Silvestri, S., Svelto, O., Lanzani, G., Cheyssac, P., and Kofman, R., 1996, *Ultrafast Phenomena* X, edited by P. F. Babara, J. G. Fujimoto, W. H. Knox and W. Zinth (Berlin: Springer).
[174] Nisoli, M., Stagira, S., de Silvestri, S., Stella, A., Togini, P., Cheyssac, P., and Kofman, R., 1997, *Phys. Rev. Lett.*, **53**, 3575.
[175] Hodak, J. K., Martini, I., and Hartland, G. V., 2000, *J. chem. Phys*, **112**, 5942.
[176] Belotskii, E., D., and Tomchuk, P. M., 1990, *Surf. Sci.*, **239**, 143.
[177] Belotskii, E., D., and Tomchuk, P. M., 1992, *Int. J. Electron.*, **73**, 955.
[178] Kurita, H., Takami, A., and Koda, S., 1998, *Appl. Phys. Lett.*, **72**, 789.
[179] Takami, A., Kurita, H., and Koda, S., 1999, *J. phys. Chem.* B, **103**, 1226.
[180] Stepanov, A. L., Hole, D. E., Bukharaev, A. A., Townsend, P. D., and Nurgazizov, N. I., 1998, *Appl. Surf. Sci.*, **136**, 298.
[181] Kamat, P. V., Flumiani, M., and Hartland, G. V., 1998, *J. phys. Chem.* B, **102**, 3123.
[182] Link, S., Burda, C., Mohamed, M. B., Nikoobakht, B., and El-Sayed, M. A., 1999, *J. phys. Chem.* A, **103**, 1165.
[183] Chang, S., Shih, C., Chen, C., Lai, W., and Wang, C. R. C., 1999, *Langmuir*, **15**, 701.
[184] Kaempfe, M., Rainer, T., Berg, K.-J., Seifert, G., and Graener, H., 1999, *Appl. Phys. Lett.*, **74**, 1200.
[185] Geohegan, D. B., Puretzky, A. A., Duscher, G., and Pennycook, S. J., 1998, *Appl. Phys. Lett.*, **72**, 2987.
[186] Lowndes, D. H., Rouleau, C. M., Thundat, T., Duscher, G., Kenik, E. A., and Pennycook, S. J., 1998, *Appl. Surf. Sci.*, **129**, 355.
[187] Sasaki, T., Terauchi, S., Koshizaki, N., and Umehara, H., 1998, *Appl. Surf. Sci.*, **129**, 398.
[188] Paszti, Z., Horvath, Z. E., Peto, G., Karacs, A., and Guczi, L., 1997, *Appl. Surf. Sci.*, **110**, 67.
[189] Lillich, H., Wolfrum, J., Zumbach, V., Aleandri, L. E., Jones, D. J., Roziere, J., Albers, P., Seibold, K., and Freund, A., 1995, *J. phys. Chem.* **99**, 12 413.
[190] Werwa, E., Seraphin, A. A., Chiu, L. A., Zhou, C. X., and Kolenbrander, K. D., 1994, *Appl. Phys. Lett.*, **64**, 1821.
[191] Lenzner, M., Krueger, J., Kautek, W., and Krausz, E., 1999, *Appl. Phys.* A, **68**, 369.
[192] Siegel, J., Ettrich, K., Welsch, E., and Matthias, E., 1997, *Appl. Phys.* A, **64**, 213.
[193] Nolte, S., Momma, C., Jacobs, H., Tuennermann, A., Chichkov, B. N., Wellegehausen, B., and Welling, H., 1997, *J. opt. Soc. Am.* B, **14**, 2716.

[194] Stuart, B. C., Feit, M. D., Herman, S., Rubenchik, A. M., Shore, B. W., and Perry, M. D., 1996, *Phys. Rev.* B, **53**, 1749.
[195] Stuart, B. C., Feit, M. D., Herman, S., Rubenchik, A. M., Shore, B. W., and Perry, M. D., 1996, *J. opt. Soc. Am.* B, **13**, 459.
[196] Kononenko, T. V., Garnov, S. V., Klimentov, S. M., Konov, V. I., Loubnin, E. N., Dausinger, F., Raiber, A., and Taut, C., 1997, *Appl. Surf. Sci.*, **109–110**, 48.
[197] Sokolowski-Tinten, K., Bialkowski, J., Cavalleri, A., von der Linde, D., Oparin, A., Meyer-ter-Vehn, J., and Anisimov, S. I., 1998, *Phys. Rev. Lett.*, **81**, 224.
[198] Link, S., Burda, C., Nikoobakht, B., and El-Sayed, M. A., 1999, *Chem. Phys. Lett.*, **315**, 12.
[199] Link, S., Burda, C., Nikoobakht, B., and El-Sayed, M. A., 2000 *J. phys. Chem.* (to be published).
[200] Link, S., Wang, Z. L., and El-Sayed, M. A., 2000 (to be published).
[201] Mirkin, C. A., Letsinger, R. L., Mucic, R. C., and Storhoff, J. J., 1996, *Nature*, **382**, 607.
[202] Andres, R. P., Bielefeld, J. D., Henderson, J. I., Janes, D. B., Kolagunta, V. R., Kubiak, C. P., Mahoney, W. J., and Osifchin, R. G., 1996, *Science*, **273**, 1690.
[203] Marinakos, S. M., Brousseau, L. C., Jones, A., and Feldheim, D. L., 1998, *Chem. Mater.*, **10**, 1214.
[204] Jensen, T. R., Schatz, G. C., and van Duyne, R. P., 1999, *J. phys. Chem.* B, **103**, 2394.
[205] Giersig, M., and Mulvaney, P., 1993, *J. phys. Chem.*, **97**, 6334.
[206] Wang, Z. L., 1998, *Adv. Mater.*, **10**, 13.
[207] Motte, L., Billoudet, F., Lacaze, E., Douin, J., and Pileni, M. P., 1997, *J. phys. Chem.* B, **101**, 138.
[208] Korgel, B. A., Fullam, S., Connolly, S., and Fitzmaurice, D., 1998, *J. phys. Chem.* B, **102**, 8379.
[209] Harfenist, S. A., Wang, Z. L., Alvarez, M. M., Vezmar, I., and Whetten, R. L., 1996, *J. phys. Chem.*, **100**, 13904.